

# We are IntechOpen, the world's leading publisher of Open Access books Built by scientists, for scientists

6,300

Open access books available

171,000

International authors and editors

190M

Downloads

Our authors are among the

154

Countries delivered to

TOP 1%

most cited scientists

12.2%

Contributors from top 500 universities



WEB OF SCIENCE™

Selection of our books indexed in the Book Citation Index  
in Web of Science™ Core Collection (BKCI)

Interested in publishing with us?  
Contact [book.department@intechopen.com](mailto:book.department@intechopen.com)

Numbers displayed above are based on latest data collected.  
For more information visit [www.intechopen.com](http://www.intechopen.com)



---

# Solar Energy Conversion and Noise Characterization in Photovoltaic Devices with Ventilation

---

Himanshu Dehra

Additional information is available at the end of the chapter

<http://dx.doi.org/10.5772/intechopen.79706>

---

## Abstract

An investigation is performed on solar energy conversion and noise characterization in photovoltaic devices with ventilation. A parallel plate photovoltaic (PV) device was installed with a pair of PV modules, a ventilated air cavity, and an insulating back panel of plywood board filled with polystyrene installed in an outdoor test room. The characterization of noise interference due to power difference of two intensities for composite waves on a PV device is presented. Standard definitions of noise sources, their measurement equations, their units, and their origins under limiting reference conditions are devised. The experiments were conducted for obtaining currents, voltages, temperatures, air velocities, sensible heat capacity, and thermal storage capacity of a PV device with active ventilation through an outdoor test room. Photovoltaic amplification was attained with power output from a potentiometer through the rotation of its circular knob. A parallel plate PV device was studied for its electrical parameters as resistance-capacitance (RC) electrical analog circuit. The effect of inductive and capacitive heating losses was considered in evaluating electrical characteristics of a PV device exposed to solar radiation. Noise filter systems as per noise sources are illustrated with examples. Some examples of noise unit calculations are tabulated based on devised noise measurement equations.

**Keywords:** solar energy conversion, PV device, photovoltaic amplification, noise characterization, ventilation, solar energy acoustics

---

## 1. Introduction

Solar energy conversion occurs at solar cells, and solar intensity of incident solar energy is converted into electric power and waste heat. The photovoltaic devices with ventilation provide means for converting waste heat lost to surrounding environment into useful thermal

power. The composite waves are transmitted in photovoltaic (PV) devices due to stresses and oscillations of incident solar and ventilation energy. In this way, solar power intensity is converted into heat, fluid, electricity, light, sound, and fire depending on intensities of its transmitted composite waves in PV devices. This chapter has summarized the concept of noise characterization in PV devices with ventilation due to solar energy conversion. The following sections define and describe noise, its sources and its measurement equations with support of experimental and numerical results of a PV device with ventilation. In order to support the noise wave characterization, signal processing is achieved from a PV device composed of RC analog signal. The noise characterization is exemplified with noise filters. Some noise unit calculations deduced from the devised noise measurement equations are also presented.

### 1.1. Noise

Noise, defined as “a sensation of unwanted intensity of a wave,” is perception of a pollutant and a type of environmental stressor. An environmental stressor such as noise may have detrimental effects on various aspects of health. The unwanted intensity of a wave is noise propagation due to transmission of waves (viz. physical agents) such as light, sound, heat, electricity, fluid, and fire. A unified theory for stresses and oscillations is applicable so as to take into effect of all the physical agents as an environmental stressor on a human body [1]. As per the theory, the stresses developed on a particle due to various forces are classified as fundamental stresses, internal stresses, and external stresses. The fundamental stresses are developed due to the presence of gravitational and electromagnetic forces of a solar system. The internal stresses are developed under the influence of fundamental stresses and are defined by properties and composition of a particle. A theory of noise interference in a wave is deemed based on noise sources and their units [1–5]. The noise sources, their measurement equations and units, are derived from the concept of interference of waves and unified theory of stresses and oscillations [6–8]. The noise filters are classified as per source signal of unwanted frequencies from solar power, electric power, light power, sound power, heat power, fluid power, and fire power [8–10]. This noise concept is also useful for characterization and checking of a human noise behavior [11].

### 1.2. Noise characterization

The interference of noise arises due to the difference of power of two intensities. The intensity of power for any particle body is a function of the development of various stresses. The phenomenon of acoustic resonance occurs when critical stress level matches with the natural stress level necessary for the oscillation of a particle body [1, 8]. The criteria for generation of acoustic resonance include waves propagated with transmission of light, sound, noise, heat, electricity, fluid, and fire from a particle body. The sensation and perception of noise from light, sound, heat, electricity, fluid, and fire is a physiological response from the sensory organs of a standard (average) human body [8].

The characterization of noise interference due to difference of power of two intensities is conceptualized. The difference of two power intensities is due to the transmission of light, sound heat, electricity, fluid, and fire into a particle body. The sources of noise are classified

according to the type of wave of interference, such as light, sound, heat, electricity, fluid, and fire. The criteria for definitions of noise are based on areas of energy stored in a wave, due to interference, speed of wave, and difference of power between two intensities of wave.

## 2. Sources of noise

The sources of noise are classified according to the type of wave of interference [3]:

**Light:** In the electromagnetic radiation wavelength band from approximately between 380 and 765 nm, the visual sensation of light is tested by the eye of an observer seeing a radiant energy. The physiological response from an average eye defines the units of light. The sensitivity of human eye is not same in all wavelengths or colors. The contribution of adding daylight is visual sensation in the visible region of the solar energy spectrum.

**Sound:** In the range of frequencies between 20 and 20,000 Hz, the sound is evaluated due to the presence of fluid pressure energy as a hearing sensation by the ear. The sound units are based on the functional feedback of an average ear. The sensitivity of sound to the whole frequency band is not the same for human ear.

**Heat:** In the electromagnetic radiation between 0.1 and 100  $\mu\text{m}$ , the heat as a temperature sensation is examined by the human body. The sensation function of temperature defines the units of heat. The temperature sensation function is a measure of coldness and hotness. The comfort zone of temperature is evaluated from functional feedback of a human body which also defines the thermal comfort. The contribution to discomfort of human body is in the ultraviolet region of solar energy spectrum.

**Electricity:** With passing of direct current or an alternating current, the electricity as a shock sensation is evaluated by skin of an observer due to the electromagnetic energy stored in a conductor which is short circuited by a human body.

**Fluid:** The fluid as combined ventilation and breathing sensation is evaluated by the amount of fluid passed either externally or internally through a standard (average) human body.

**Fire:** The exposure of radiant energy and fluid acting on the skin surface of an average human body defines the fire as a sensation of burning.

## 3. Definitions

The definitions of noise sources are characterized by energy area stored in a wave with its speed and difference due to power intensities of two waves due to the interference [8].

**Noise of sol:** The difference of power intensities between two solar power systems causes noise of sol (S). The power storage on a unit area per unit time defines the amplitude of a solar energy wave.

The storage of solar power is defined by a solar energy wave pack of unit cross sectional area and of length  $s$ , the velocity of light.

**Noise of therm:** The difference of power intensities between two heat power systems causes noise of therm. The power storage on a unit area per unit time defines the amplitude of a heat wave.

The storage of heat power is defined by the heat energy wave pack of unit cross sectional area and of length  $s$ , the velocity of light.

**Noise of photons:** The difference of power intensities between two lighting power systems causes noise of photons. The power storage on a unit area per unit time defines the amplitude of a light beam.

The storage of light beam is defined by the light beam packet of unit cross sectional area and of length  $s$ , the velocity of light.

**Noise of electrons:** The difference of power intensities between two electrical power systems causes noise of electrons. The power storage on a unit area per unit time defines the amplitude of an electricity wave.

The storage of electrical power is defined by an electricity wave pack of unit cross sectional area and of length  $s$ , the velocity of light.

**Noise of scattering:** The difference of power intensities between two fluid power systems causes noise of scattering. The power storage on a unit area per unit time defines the amplitude of a fluid wave.

The storage of fluid power is defined by the fluid energy wave pack of unit cross sectional area and of length  $s$ , the velocity of fluid.

**Noise of scattering and lightning:** The difference of power intensities between two fire power systems causes noise of scattering and lightning. The power storage on a unit area per unit time defines the amplitude of a fire flash.

The storage of fire power of light is defined by the fire pack of unit cross sectional area and of length  $s$ , the velocity of light. The storage of fire power of fluid is defined by the fire pack of unit cross sectional area and of length  $s$ , the velocity of fluid.

**Noise of elasticity:** The difference of power intensities between two sound power systems causes noise of elasticity. The power storage on a unit area per unit time defines the amplitude of a sound wave. The storage of sound power is defined by the sound energy wave pack of unit cross sectional area and of length  $s$ , the velocity of sound.

#### 4. Noise measurement equations

The following standard measurement equations are derived and adopted from the standard definitions for sources of noise interference as mentioned in previous sections [8, 9].

**Noise of sol:** For a pack of solar energy wave, the multiplication of solar power storage and the velocity of light give solar power intensity  $I$ . On taking logarithm of two intensities of solar power,  $I_1$  and  $I_2$ , provides intensity difference. It is mathematically expressed as [8]:

$$Sol = \log(I_1)(I_2)^{-1} \quad (1)$$

But, the logarithmic unit ratio for noise of sol is expressed as  $Sol$ . The oncosol ( $oS$ ) is more convenient for solar power systems. The mathematical expression by the following equality gives an oncosol ( $oS$ ), which is 1/11th unit of a  $Sol$  [8]:

$$oS = \pm 11 \log(I_1)(I_2)^{-1} \quad (2)$$

**Noise of therm:** For a pack of heat energy wave, the multiplication of the total power storage and the velocity of light gives heat power intensity  $I$ . The pack of solar energy wave and heat energy wave (for the same intensity  $I$ ) have same energy areas; therefore, their units of noise are the same as  $Sol$ .

**Noise of photons:** For a pack of light energy beam, the multiplication of the total power storage and the velocity of light gives light power intensity  $I$ . The pack of solar energy wave and light energy beam (for the same intensity  $I$ ) have same energy areas; therefore, their units of noise are the same as  $Sol$ .

**Noise of electrons:** For a pack of electricity wave, the multiplication of the total electrical storage and the velocity of light gives electrical power intensity  $I$ . The pack of solar energy wave and electricity wave (for the same intensity  $I$ ) have same energy areas; therefore, their units of noise are the same as  $Sol$ .

**Noise of scattering:** For a pack of fluid energy wave, the multiplication of the total power storage and the velocity of fluid gives fluid power intensity  $I$ . On taking logarithm of two intensities of fluid power,  $I_1$  and  $I_2$ , provides intensity difference. It is mathematically expressed as [8]:

$$Sip = \log(I_1)(I_2)^{-1} \quad (3)$$

But, the logarithmic unit ratio for noise of scattering is  $Sip$ . The oncisip ( $oS$ ) is more convenient for fluid power systems.

The mathematical expression by the following equality gives an oncisip ( $oS$ ), which is 1/11th unit of a  $Sip$  [8]:

$$oS = \pm 11 \log(I_1)(I_2)^{-1} \quad (4)$$

For energy area determination for a fluid wave, the water with a specific gravity of 1.0 is the standard fluid considered with a power of  $\pm 1 \text{ W m}^{-2}$  for a reference intensity  $I_2$ .

**Noise of scattering and lightning:** For a pack of fire wave, the intensity,  $I$ , of fire flash with power of light is the multiplication of the total power storage and the velocity of light. Whereas

for a pack of fire wave, the intensity,  $I$ , of fire flash with power of fluid is the multiplication of the total power storage capacity and the velocity of fluid.

For a noise due to fire flash, the collective effect of scattering and lightning is to be obtained by the superimposition principle.

- For the same intensity  $I$ , the pack of solar energy wave and a fire flash with light power has the same energy areas; therefore, their units of noise are the same as *Sol*. The therm power may also be included in fire flash with power of light.
- For the same intensity  $I$ , the pack of fluid energy wave and a fire flash with fluid power has the same energy areas; therefore, their units of noise are same as *Sip*. In determining the areas of energy for the case of fluids other than water, a multiplication factor in specific gravity of fluid is to be considered.

**Noise of elasticity:** For a pack of sound energy wave, the product of the total power storage and the velocity of sound gives sound power intensity  $I$ . On taking logarithm of two intensities of sound power,  $I_1$  and  $I_2$ , provides intensity difference. It is mathematically expressed as [8]:

$$Bel = \log(I_1)(I_2)^{-1} \quad (5)$$

But, the logarithmic unit ratio for noise of elasticity is *Bel*. The oncibel (oB) is more convenient for sound power systems. The mathematical expression by the following equality gives an oncibel (oB), which is 1/11th unit of a *Bel* [8]:

$$oB = \pm 11 \log(I_1)(I_2)^{-1} \quad (6)$$

There are following elaborative points on choosing an *onci* as 1/11th unit of noise [11]:

Reference value used for  $I_2$  is  $-1 \text{ W m}^{-2}$  on positive scale of noise and  $1 \text{ W m}^{-2}$  on negative scale of noise. In a power cycle, all types of wave form one positive power cycle and one negative power cycle (see **Figure 10**). Positive scale of noise has ten positive units and one negative unit, whereas the negative scale of noise has one positive unit and ten negative units:

- Each unit of *sol*, *sip*, and *bel* is divided into 11 parts, 1 part is 1/11th unit of noise, and
- The base of logarithm used in noise measurement equations is 11.

The reference value of  $I_2$  is  $-1 \text{ W m}^{-2}$  with  $I_1$  on positive scale of noise, should be taken with negative noise measurement expression (see Eqs. (2), (4) and (6)); therefore, it gives positive values of noise.

The reference value of  $I_2$  is  $1 \text{ W m}^{-2}$  with  $I_1$  on negative scale of noise, should be taken with positive noise measurement expression (see Eqs. (2), (4) and (6)); therefore, it gives negative values of noise.

Some noise unit calculation examples are illustrated later in this chapter.

#### 4.1. Limiting conditions and reference values

**Table 1** has summarized the units of noise and their limiting conditions [3].

Reference*	Noise scales and limiting conditions		
$I_2 = \pm 1 \text{ W m}^{-2}$	Noise of sol	Noise of scattering	Noise of elasticity
Units	Sol	Sip	Bel
$I_1 = 1 \text{ W m}^{-2}$	No positive solar energy	No positive fluid energy	No positive sound energy
$I_1 = 1+ \rightarrow 0 \text{ W m}^{-2}$	Decreasing solar energy	Decreasing fluid energy	Decreasing sound energy
$I_1 = +ve$	Increasing solar energy	Increasing fluid energy	Increasing sound energy
$I_1 = -1 \text{ W m}^{-2}$	Negative solar energy	Negative fluid energy	Negative sound energy
	Darkness	Low pressure	Inaudible range
$I_1 = -ve$	Darkness increasing, distance from point source of light increasing	Low pressure increasing, vacuum approaching	Inaudible range increasing, vacuum approaching
$I_1 = -1+ \rightarrow 0 \text{ W m}^{-2}$	Negative solar energy	Negative fluid energy	Negative sound energy
	Decreasing darkness	Decreasing low pressure	Decreasing inaudible range

\*Reference value of  $I_2 = \pm 1 \text{ W m}^{-2}$  signifies the limiting condition with areas of noise interference approaching to zero.

Table 1. Noise under limiting conditions.

## 5. Noise filter systems

The criteria for definitions of filters for noise filtering are based on the areas of energy stored in a wave due to the noise interference, speed of wave, and difference of power between two intensities of wave [8]. The filtered noise signals are considered from systems of solar power, electric power, light power, sound power, heat power, fluid power, and fire power. The noise filters as per sources of noise are defined as follows [8]:

**Filter for noise of sol:** This filter is used to filter noise due to the difference of intensities of power between two solar power systems. Example: window curtain, window blind, wall, and sunglasses.

**Filter for noise of therm:** This filter is used to filter noise due to the difference of intensities of power between two heat power systems. Example: house, insulation, clothing, and furnace.

**Filter for noise of photons:** This filter is used to filter noise due to the difference of intensities of power between two lighting systems. Example: 3-D vision of any object, electric bulb, television, computer, and LCD screen laptop.

**Filter for noise of electrons:** This filter is used to filter noise due to the difference of intensities of power between two electrical power systems. Example: AM/FM radio clock with ear phones, telephone instrument with ear phones, and CD audio player with ear phones.

**Filter for noise of scattering:** This filter is used to filter noise due to the difference of intensities of power between two fluid power systems. Example: electric fan, pump, motor vehicle, river stream, rain, and tap water.

**Filter for noise of scattering and lightning:** This filter is used to filter noise due to the difference of intensities of power between two fire power systems. Example: lighter, matchstick, gas stove, locomotive engine, and thunderbolt.

**Filter for noise of elasticity:** This filter is used to filter noise due to the difference of intensities of power between two sound power systems. Example: human vocal chords, organ pipe, thunderbolt, and drum beats.

### 5.1. Some examples of noise filters

Some examples of noise filters are enumerated as under [10]:

**Human voice production:** The example of phonetics of filtering sound of a human speech is illustrated. The human speech is synthesized due to the development of stresses at vocal folds. The smoothening of the sound is a function of its amplitude and its shape of oscillations at vocal tract of a human being. The vocal tract is a resonant cavity wall with sound energy stored in oscillations of its vocal folds. The vocal apparatus showing the mechanism of synthesis of human speech is illustrated in **Figure 1**.

**An airflow window with a photovoltaic solar wall:** The filtering of solar energy is illustrated through an example of an airflow window attached with a shading device. An airflow window is fixed with a movable roller blind to control the transmission of daylight as well as the amount of solar heat. The bottom portion of photovoltaic solar wall is used for controlling the amount of air ventilation along with the generation of solar electric power. The example is illustrated in **Figure 2**.

**Psychrometric air conditioner:** An elementary air conditioner for summer comfort conditioning consists of a cooling coil, a cooling fluid with a filter. The schematic of operation of a psychrometric air conditioner is illustrated in **Figure 3**.

**Telephone line:** The impedance of a telephone line is composed of distributed resistance, capacitance, and inductance. The impedance of telephone line is proportional to the insulation, loop length, and whether the wire is buried, aerial or bare parallel wires strung on

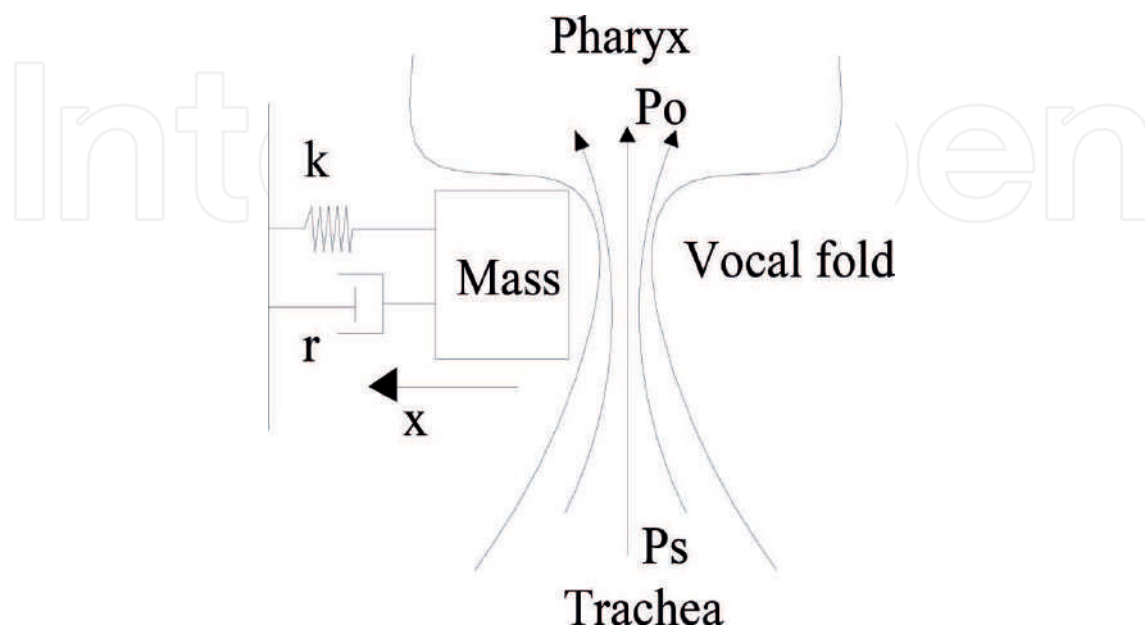


**Figure 1.** A human vocal mechanism.

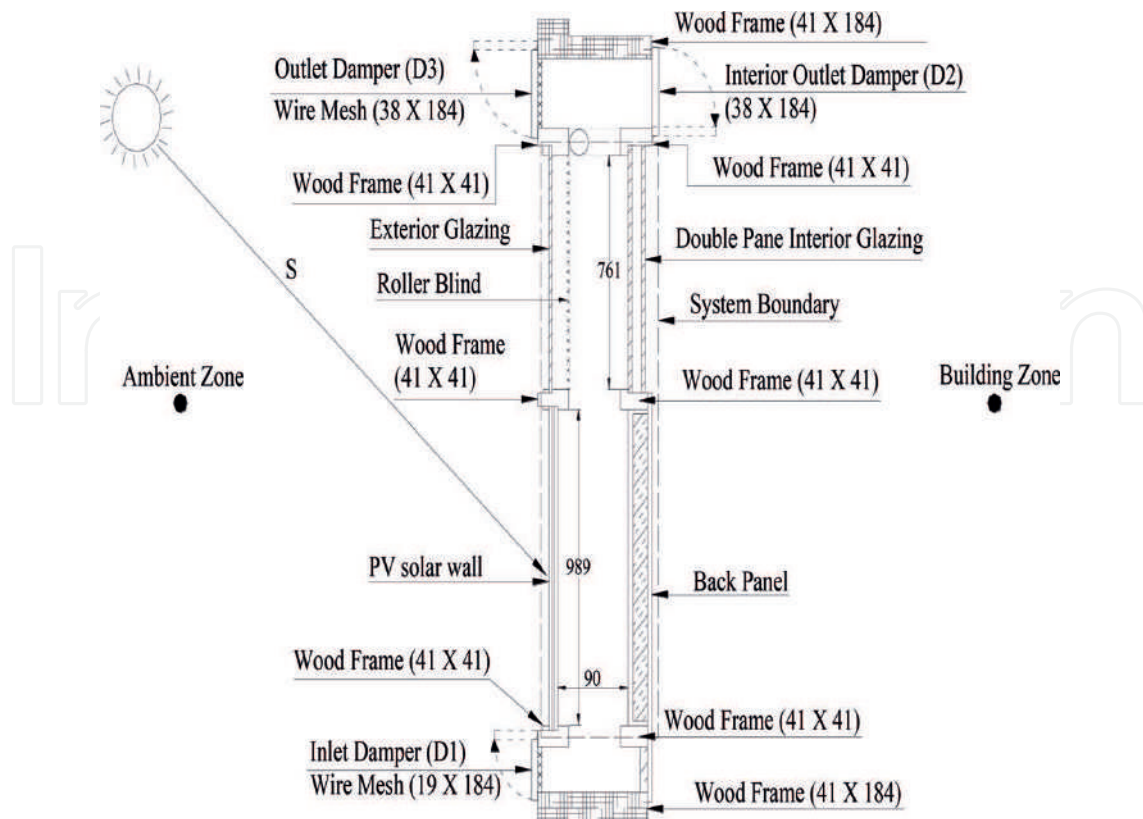


Figure 2. An airflow window with a photovoltaic solar wall (dimensions shown are in mm).

telephone pole. A telephone line is usually supplied with a 48 VDC from the telephone exchange. The schematic of operation of a telephone line with telephone instrument is illustrated in Figure 4.

**Fire and smoke detection system:** A fire detection system consists of a control system with interconnected alarms, smoke, and heat detectors. A fire detector is a device which is used for presetting an alarm at a particular temperature. A smoke detector is a device which is used for presetting an alarm when a certain percentage of smoke accumulates. The photovoltaic cell activates the smoke alarm only if it senses requisite obscuration of light over a unit area with control from BMS. The schematic of various components for fire detection system is illustrated in Figure 5.

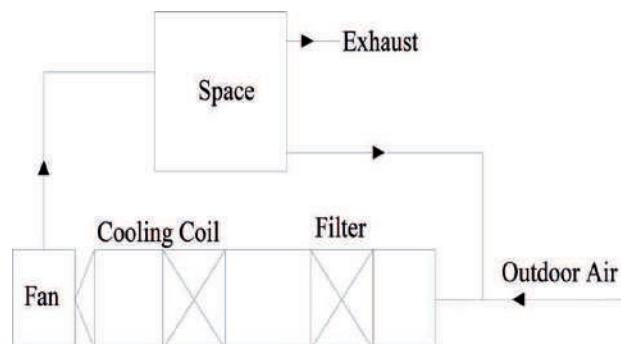


Figure 3. A psychrometric air conditioner.

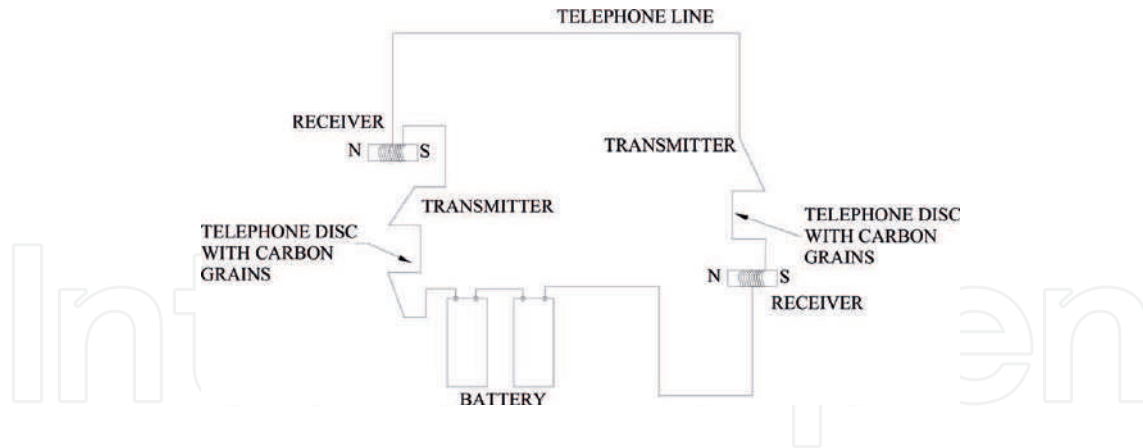


Figure 4. Operation of a telephone line.

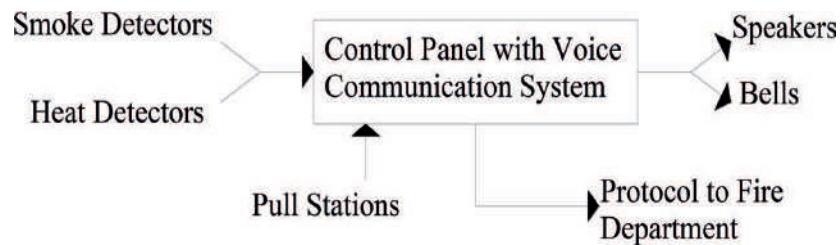
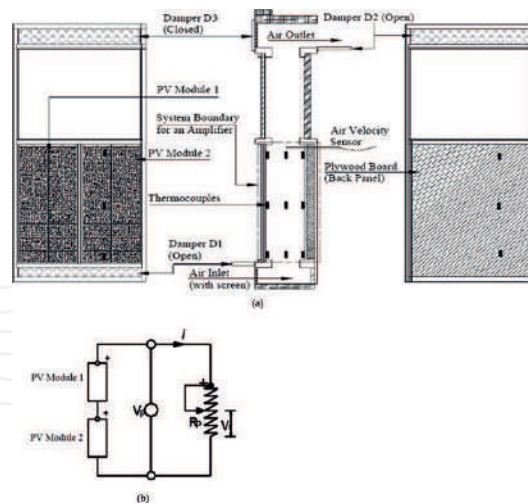


Figure 5. A fire detection system.

## 6. Experimental and numerical results

The full scale experimental setup for a parallel plate photovoltaic device connected to a potentiometer was installed in an outdoor room facility located at Concordia University, Montréal, Québec, Canada [12–23]. The schematic of the experimental setup is illustrated in **Figure 6**. An amplifier was built with a pair of photovoltaic (PV) modules forming a parallel plate channel with a plywood board and connected to a potentiometer. A potentiometer, a wire-wound variable resistor of up to  $50\ \Omega$ , was a wire-wound circular coil with a sliding knob contact [23]. It was used to vary electrical resistance across connected PV modules without interrupting the current. The characteristics of a parallel plate photovoltaic device connected to a potentiometer were established by varying electrical resistance with the rotation of knob of a potentiometer. The current-voltage measurements were obtained for determining electric power output with a series electrical circuit connection of a pair of vertically inclined PV modules installed on a wooden frame.

The temperatures were measured as a function of volume of a parallel plate photovoltaic device. The nonlinear thermal results include measurements of temperatures for PV modules, insulating panel, and ventilated air column in the wooden frame. The air velocities were developed in the ventilated air column for the transportation of heat both as a measure of buoyancy and fan induced ventilation. The electrical measurement results of currents, voltages, and power with varying electrical resistance of potentiometer are presented in **Table 2**. The thermal measurement results of temperatures of various components of PV device, ambient air and room air temperatures, air velocities and solar intensities are presented in **Table 3**. The location and nomenclature of sensors are presented in **Table 4**. The results of the power output from a potentiometer with the rotation of circular knob are illustrated in **Figure 7**.



**Figure 6.** Schematic of experimental setup for a parallel plate photovoltaic device connected to a potentiometer: (a) location of sensors; and (b) electrical circuit diagram.

A simulation model for the prediction of temperature distributions varying with the volume of a parallel plate photovoltaic device was developed. The model was used to predict the temperature distributions at pre-defined locations in PV module, plywood board, and air flowing through a parallel plate channel through the walls of vertically inclined photovoltaic modules. The model results of the temperature plots are illustrated in **Figure 8(a)–(c)**. Some noise unit examples for an air duct exposed to solar radiation are illustrated in **Tables 5–8**. These tables have shown noise unit calculations on positive scale of noise.

### 6.1. Photovoltaic amplification

The phenomenon of photovoltaic amplification is observed from the graphs of **Figures 7 and 8** [21]. The gain in steady state electrical and thermal functions for a photovoltaic device is a factor of its volume or resistance. This operational characteristic is similar to the operation of a loudspeaker. The electrical analog is used to describe the resonance phenomenon for

Rotation	Volts	Amps	Watts	Rotation	Volts	Amps	Watts	Rotation	Volts	Amps	Watts
240°	18.7	—	—	83°	16.3	0.935	15.23	30°	9.7	1.577	15.21
239°	16.5	0.331	5.461	75°	16.0	1.014	16.26	27°	9.0	1.587	14.33
201°	17.4	0.414	7.195	69°	15.8	1.100	17.38	21°	7.1	1.583	11.24
185°	17.5	0.454	7.940	64°	15.5	1.165	18.04	18°	6.2	1.573	9.831
162°	17.3	0.513	8.885	55°	15.0	1.302	19.53	17°	5.7	1.578	9.026
150°	17.18	0.550	9.449	50°	14.5	1.386	20.05	12°	3.9	1.567	6.257
142°	17.19	0.582	10.00	43°	13.2	1.503	19.79	10°	3.2	1.553	4.840
128°	17.1	0.640	10.93	42°	13.1	1.493	19.49	1.5°	0.5	1.593	0.807
107°	16.8	0.750	12.51	37°	11.9	1.536	18.26	1°	0.3	1.59	0.426
89°	16.4	0.884	14.45	32°	10.5	1.567	16.42	0°	—	1.643	—

**Table 2.** Sample electrical measurement results of a PV device with varying resistance of potentiometer.

Run no.	S (W m <sup>-2</sup> )	Ep (W)	To (°C)	Ts (°C)	v (m s <sup>-1</sup> )	T <sub>p</sub> (b) (°C)	T <sub>p</sub> (m) (°C)	T <sub>p</sub> (t) (°C)	T <sub>b</sub> (b) (°C)	T <sub>b</sub> (m) (°C)	T <sub>b</sub> (t) (°C)	T <sub>a</sub> (b) (°C)	T <sub>a</sub> (m) (°C)	T <sub>a</sub> (t) (°C)
1	697.5	31.0	13.5	22.1	0.451	34.5	33.01	36.2	20.2	24.4	27.6	18.7	19.3	22.5
2	725.4	31.1	15.9	22.9	0.362	32.5	33.3	35.7	20.2	23.9	29.1	18.3	19.7	23.3

Table 3. Sample thermo-fluid measurement results.

Locations shown in Figure 1	T <sub>p</sub> (b) (°C)	T <sub>p</sub> (m) (°C)	T <sub>p</sub> (t) (°C)	T <sub>b</sub> (b) (°C)	T <sub>b</sub> (m) (°C)	T <sub>b</sub> (t) (°C)	T <sub>a</sub> (b) (°C)	T <sub>a</sub> (m) (°C)	T <sub>a</sub> (t) (°C)	Air velocity sensor
y (cm)	15	55	94	15	55	94	15	55	94	99
Z (cm)	60	60	60	60	60	60	60	60	60	60
X (mm)	6.2	6.2	6.2	96.2	96.2	96.2	51.2	51.2	51.2	51.2

Note: x is horizontal; y is vertical; and z is adjacent 3rd axis of x-y plane.

Table 4. Nomenclature and location of sensors.

equivalent mechanical, hydraulic, and thermal systems of a parallel plate photovoltaic device connected to a potentiometer. Figure 9(a) and (b) shows series and parallel cases of L-C-R arrangement of resonance, respectively.

### 6.2. Signal processing: electrical parameters for a PV device

The sinusoidal steady-state response was applied in performing the analysis of the parallel plate PV device circuit, because of the advantage of representing a periodic function in terms of a sinusoidal exponential function. Electrical analog RC circuit parameters of a parallel plate PV device are enumerated as under [2, 13]:

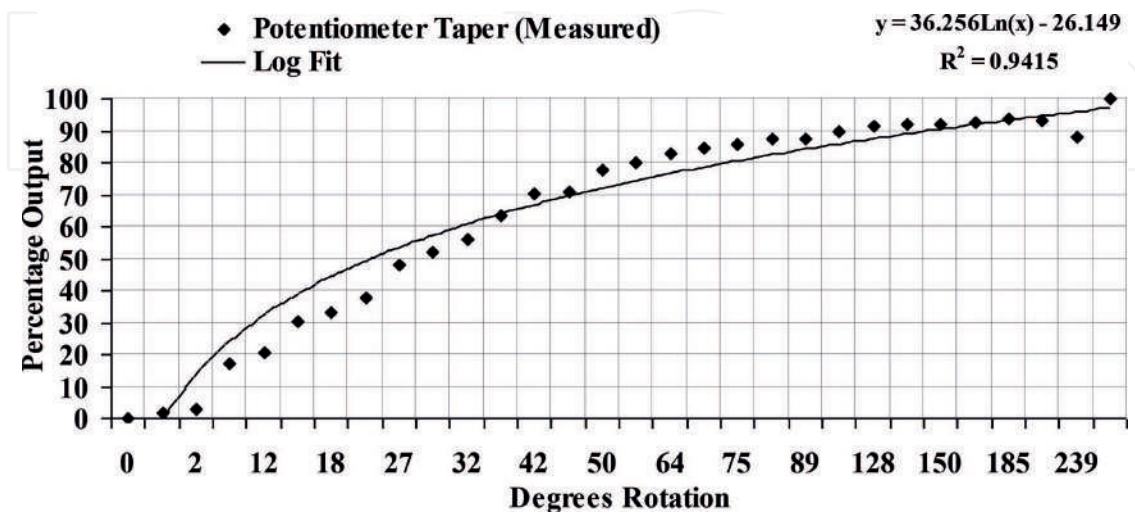


Figure 7. Potentiometer taper (measured) with percentage voltage output.

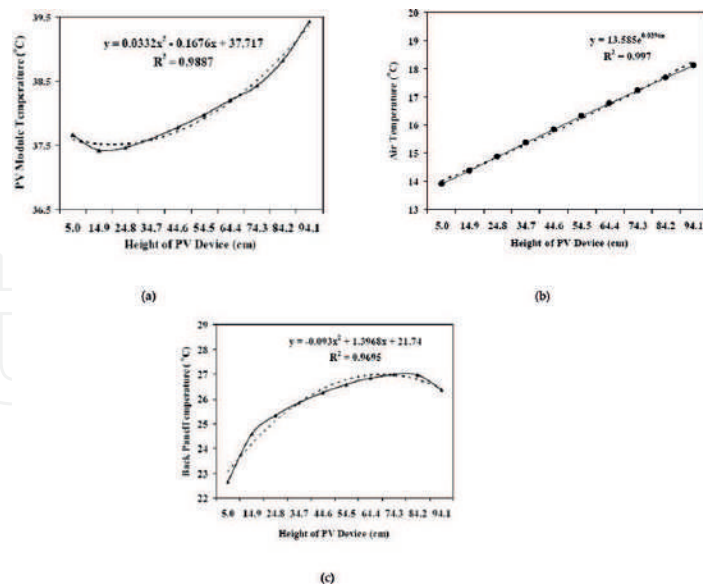


Figure 8. Temperature plots with height of a PV device: (a) PV module; (b) air; and (c) plywood board.

Solar irradiation ( $W\ m^{-2}$ )	Air temperature difference ( $\Delta T$ ) ( $^{\circ}C$ )	Noise of Sol oS (oncisol)
450	15.50	28
550	18.90	28.93
650	22.40	29.7
750	25.90	30.36
850	29.40	30.91

Table 5. Temperature difference and noise of sol with solar irradiation (air velocity:  $0.75\ m\ s^{-1}$ ).

Air velocity ( $m\ s^{-1}$ )	Fluid power ( $W\ m^{-2}$ )	Air temperature difference ( $\Delta T$ ) ( $^{\circ}C$ )	Noise of scattering oS (oncisp)
1.35	47.62	15.28	17.72
1.05	37.0	18.22	16.50
0.75	26.45	22.40	15.02
0.45	15.87	28.15	12.65
0.15	05.29	29.80	07.64

Table 6. Temperature difference and noise of scattering with air velocity ( $S = 650\ W\ m^{-2}$ ).

**Capacitance:** The capacitance of a parallel plate PV device with air as a dielectric medium was calculated to be 91.2 picofarads.

( $\Delta T$ ) °C	Mass flow rate (kg s <sup>-1</sup> )	Thermal power (W m <sup>-2</sup> )	Noise of therm oS (oncisol)	( $\Delta T$ ) (°C)	Mass flow rate (kg s <sup>-1</sup> )	Thermal power (W m <sup>-2</sup> )	Noise of therm oS (oncisol)
15.50	0.01376	71.09	19.5602	15.28	0.0231	117.65	21.868
18.90	0.01275	80.325	20.119	18.22	0.0171	103.85	21.296
22.40	0.0120	89.6	20.614	22.40	0.0120	89.6	20.614
25.90	0.0115	99.2833	21.043	28.15	8.1 X 10 <sup>-3</sup>	76.0	19.866
29.40	0.0111	108.78	21.505	29.80	6.2 X 10 <sup>-3</sup>	61.59	18.898

Table 7. Mass flow rate and noise of therm with ( $\Delta T$ ) (°C).

Air velocity (m s <sup>-1</sup> )	Fluid power (W m <sup>-2</sup> )	Noise of scattering oS (oncisp)	Sound pressure (N m <sup>-2</sup> )	Sound power intensity (W m <sup>-2</sup> )	Noise of elasticity oB (oncibel)
1.35	47.62	17.72	557.5	752.7	30.36
1.05	37.0	16.50	433.65	455.33	28.05
0.75	26.45	15.02	309.75	232.31	24.97
0.45	15.87	12.65	185.85	83.63	20.24
0.15	05.29	07.64	61.94	09.29	10.12

Table 8. Noise of elasticity with air particle velocity (impedance  $Z_0 = 413 \text{ N s m}^{-3}$  at 20°C).

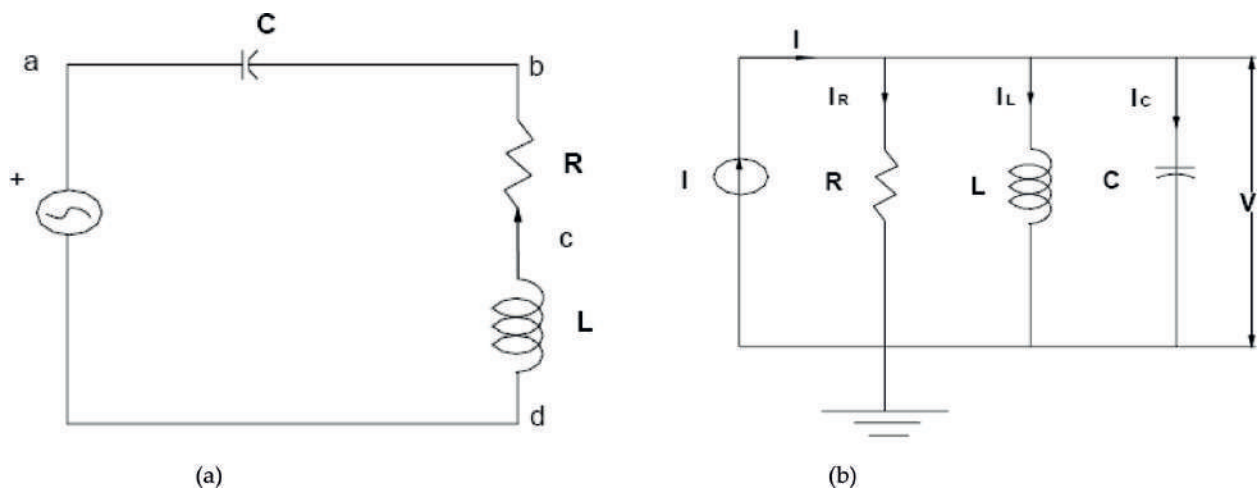


Figure 9. (a) L-C-R series arrangement of resonance and (b) L-C-R parallel arrangement of resonance.

**Resistance:** The electrical resistances of various components were calculated as: glass coated PV modules were approximated as 5.3 kΩ, air was approximated as 1200 MΩ, and plywood board was approximated as 26.5 Tera Ω. The total equivalent electrical resistance of a parallel plate PV solar wall device was approximated as 5.3 kΩ.

**Time constant:** The time constant, which is a product of resistance and capacitance, was calculated to be:  $0.5 \mu\text{s}$ . The frequency with this time constant was calculated to be 2 MHz.

**Capacitive reactance:** The capacitive reactance was calculated to be  $872.5 \Omega$ .

**Impedance:** The impedance of the circuit was calculated to be  $5.4 \text{ k}\Omega$ .

**The phase angle  $\theta$ :** The phase angle between capacitance and reactance was calculated to be  $9^\circ$ .

*The phasor representation:*

$$Z = 5.300 - j0.8725 = 5.4 \text{ k}\Omega \angle -9^\circ.$$

**Capacitive heating:** The joule law gives instantaneous power absorbed by the capacitive impedance which is converted into heat. The heat capacities under critical operation of buoyancy-induced ventilation were calculated to be 59.6, 0.755, and 510.7 for PV module, air, and plywood board, respectively. The total average value of joule heating for the parallel plate PV device was calculated to be 571 kJ.

**Induction losses:** The induction losses due to the thermal storage effect in the parallel plate PV device were calculated to be 15.9 kJ.

**Power factor:** The power factor was calculated to be  $\cos\theta = 0.911$  lag.

**Current function ( $i^2(t)$ ):** Using the current function,  $i^2(t) = I_m^2 \sin^2(\omega t + \theta)$ , the effective (root mean square) value of current was calculated to be 10.4 amps, and the maximum value of current was calculated to be 14.71 amps.

**Voltage function:** The voltage function is defined as per the sine wave:  $v = V_m \sin(\omega t)$ . The effective value of the voltage was calculated to be 60.4 V, and the maximum value of the voltage was calculated to be 85.42 V.

**Power function:** The instantaneous power is given by the expression [2]:

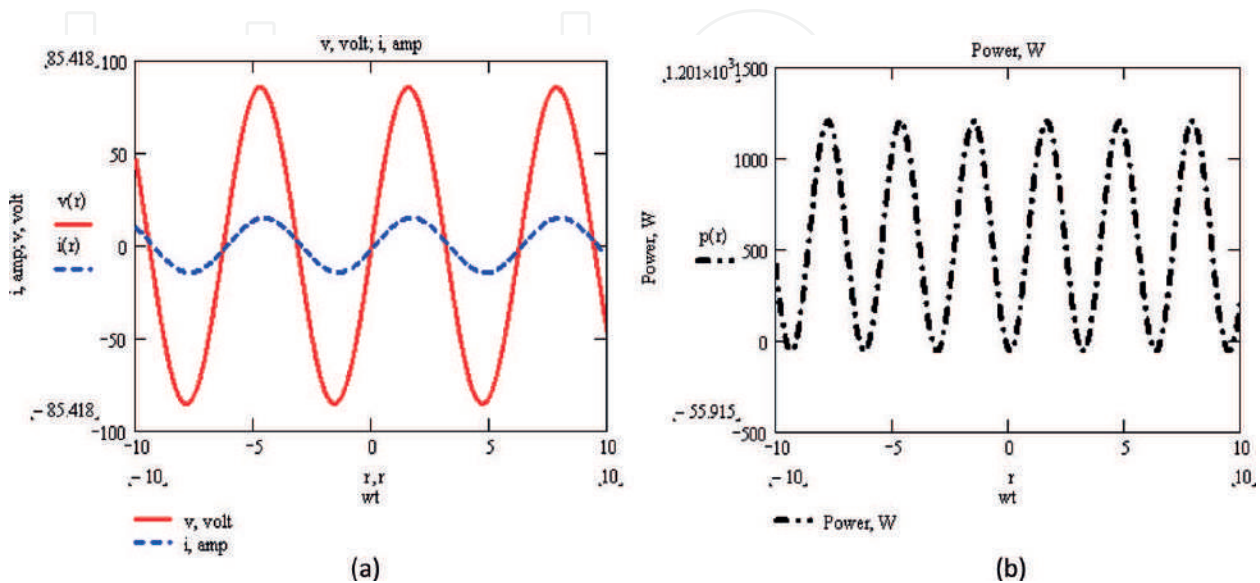


Figure 10. Time diagrams: (a) voltage and current and (b) power in a RC circuit amplifier.

$$p(t) = \frac{V_m I_m}{2} \cos(\theta) - \frac{V_m I_m}{2} \cos(2\omega - \theta) \quad (7)$$

**The plots:** The time diagram for current and voltage is plotted in **Figure 10(a)**. The time diagram for power is plotted in **Figure 10(b)**.

**Power transfer:** **Figure 10** shows that the instantaneous power is negative whenever the voltage and current are of opposite sign. However, as is illustrated in **Figure 10** that positive area of  $p(t)$  energy exceeds the negative area. Therefore, the average power is finite. Since the angle,  $\theta$ , is small between current and voltage, the negative area of energy becomes very small. During the first quarter cycle (from  $0^\circ$  to  $90^\circ$ ), the applied voltage rises from slightly negative value to a maximum, and the capacitor is receiving a charge. The power curve is positive during this period and represents energy stored in the capacitor. From  $90^\circ$  to  $180^\circ$ , the applied voltage is falling from maximum to slightly negative value, and the capacitor is discharging. The corresponding power curve is negative and represents energy returned to the circuit during this interval. The third quarter cycle represents a period of charging the capacitor, and the fourth quarter represents a discharge period. The induction losses are due to the thermal storage amount to 1.5% in comparison to the capacitive heating. Thus, induction losses cannot be avoided in any electrical circuit, but can be minimized.

## 7. Discussion

The following composite waves are generated due to the development of stresses and oscillations on a PV solar wall device with incident short wavelength electro-magnetic waves [1]: (i) due to the connected external electrical load and transmission of electrical energy wave; (ii) due to the exchange of viscous dissipation with air and the propagation of heat waves at longer wavelength; (iii) due to the thermal stress generation with propagation of heat waves, and elastic waves are transmitted in a PV solar wall device; (iv) due to the combination of stress development with heat waves, elastic waves, and applied external source of energy, and the fluid surface waves are propagated; and (v) due to the climate particle oscillations of wind and fan induced pressure, and applied external waves are propagated; in the absence of wind and fan pressure, thermosyphon-based oscillations are propagated due to the thermal buoyancy [18, 23].

Such as in an organ pipe, the sound waves can transmit with the combination of applied external source of energy and fluid surface waves. From the surrounding environment due to air-borne sound transmission, the sound waves are propagated. Due to various stresses and oscillations acting on a static particle body, the transmission of composite waves is generated. With the action of composite forces acting on a PV solar wall device, the developed stresses are classified as: (i) fundamental; (ii) internal; and (iii) external. Due to the presence of electromagnetic and gravitational forces of a solar system, the fundamental stresses are generated. Under the influence of fundamental stresses, internal stresses are generated with characterization of composition properties at chemical, atomic, and molecular level. With application of external source of energy such

as fan-based force used for active air ventilation in PV solar wall device, the external stresses are generated. With stress development due to the periodic force of expansion/compression, cooling/heating and night/day, the oscillations are assumed to be generated on the PV solar wall device. On a PV solar wall device, climate particle oscillations due to wind force are also transmitted. Due to the superposition of composite waves, the fluctuating forces are generated.

**Resonance:** The parallel and series cases of LCR circuit resonance are briefed here [8, 10]. With the aid of presented modeling and experimental data, the cases of resonance are visualized. For elastic waves transmission, the inductance force exists due to the mass of the mechanical system. The capacitance force exists due to the heat storage capacities of PV solar wall device (PV modules, air, and polystyrene filled plywood board). The polystyrene filled plywood board is vulnerable to heat stress of fire as soon as heat waves propagated with frequency matching with its latent heat of vaporization is achieved. Due to the thermal and fluid resistance in energy storage elements of the PV solar wall device, equivalent electrical analog resistance is developed. The parallel case of LCR resonance happens with fluid surface waves (RC) and heat waves (RC) in conjunction with inductance (L) due to the mass of PV solar wall device and resistance (R) due to temperatures of ambient air and ground surface. The series case of LCR resonance occurs with propagation of elastic waves of a PV solar wall device.

## 8. Conclusion

A study on solar energy conversion and noise characterization in photovoltaic devices with ventilation is performed. The noise interference and characterization as per speed of a composite wave are presented. The sources of noise waves (sun, light, sound, heat, electricity, fluid, and fire) are described depending on their speed of noise interference. Noise measurement equations and their units are coined. The power systems are classified as per source signals of solar power, electric power, light power, sound power, heat power, fluid power, and fire power. The noise filters for filtering noise from power systems are defined with examples. The experimental results along with results of the simulation model for noise filtering for a PV device are presented. Some noise unit examples for an air duct exposed to solar radiation are illustrated. A phenomenon of photovoltaic amplification for a pair of photovoltaic modules connected to a potentiometer is explained. The time plots of power function were used to support and devise noise measurement expressions and noise characterization in a power system as per speed of a wave.

## Author details

Himanshu Dehra

Address all correspondence to: [anshu\\_dehra@hotmail.com](mailto:anshu_dehra@hotmail.com)

Egis Group, Gurugram, Haryana, India

## References

- [1] Dehra H. A unified theory for stresses and oscillations. In: Proc. CAA Conf., Montréal 2007 Canada, Canadian Acoustics. Vol. 35(3). 2007. pp. 132-133
- [2] Dehra H. Power transfer and inductance in a star connected 3-phase RC circuit amplifier. In: Proc. AIChE 2008 Spring Meeting, New Orleans, LA, USA. Session 96a. 2008. 7 p
- [3] Dehra H. The noise scales and their units. In: Proc. CAA Conf., Vancouver 2008 Canada, Canadian Acoustics. Vol. 36(3). 2008. pp. 78-79
- [4] Dehra H. A benchmark solution for interference of noise waves. In: Proc. AIChE Spring 2009; Tampa, FL, USA; April 26-30, Session 67c. 2009. 4 p
- [5] Dehra H. Solar energy absorbers. In: Manyala R editor. Chapter 6 in Solar Collectors and Panels, Theory and Applications. Intech Publication; 2010. pp. 111-134
- [6] Dehra H. A theory of acoustics in solar energy. Natural Resources. 2013;4(1A):116-120
- [7] Dehra H. A slide rule for noise measurement. In: 10th International Conference on Sustainable Energy Technologies (SET 2011); Istanbul, Turkey; September 4-7. 2011. 5 p
- [8] Dehra H. A novel theory of psychoacoustics on noise sources, noise measurements and noise filters. In: Proc. NoiseCon16 Conf.; 13-15 June; Providence, Rhode Island, USA. 2016. pp. 933-942
- [9] Dehra H. On sources and measurement units of noise. In: Proc. International Conference on Innovation, Management and Industrial Engineering (IMIE 2016); 05-07 August 2016; Kurume, Fukuoka, Japan; 2016. pp. 219-227. ISSN: 2412-0170
- [10] Dehra H. Acoustic filters. In: Romano VA, Duval AS, editors. Chapter 5 in Ventilation: Types, Standards and Problems. New York, USA: Nova Science Publishers; 2011. 245 pp. ISBN: 978-1-62618-281-3
- [11] Dehra H. A paradigm for characterization and checking of a human noise behavior. In: WASET Proceedings of 19th International Conference on Psychological and Brain Sciences; May 11-12, 2017; Montréal, Canada. pp. 317-325. <http://waset.org/publications/10007615>
- [12] Dehra H. Photovoltaic solar wall: 2-D numerical modeling and experimental testing under fan induced hybrid ventilation. In: Proceedings of the IEEE International Conference on Energy Efficient Technologies for Sustainability, April 7-8. IEEE Xplore, ISBN: 978-1-4673-9925-8; 2016. pp. 668-676
- [13] Dehra H. A multi-parametric PV solar wall device. In: Proceedings of IEEE International Conference on Power, Control, Signals and Instrumentation Engineering (ICPCSI-2017), 978-1-5386-0814-2/17/\$31.00 ©2017 IEEE, Chennai, India on 21-22 Sep 2017
- [14] Dehra H. Characterization of noise in power systems. In: Proceedings of IEEE International Conference on Power Energy, Environment & Intelligent Control (PEEIC2018), 978-1-5386-2341-1/18/\$31.00 ©2018 IEEE, Greater Noida, India on April 13-14, 2018. pp. 321-330

- [15] Dehra H. A guide for signal processing of sensors and transducers. In: Proc. AIChE 2009 Spring Meeting; Tampa, FL, USA. 2009. Session 6b
- [16] Dehra H. A numerical and experimental study for generation of electric and thermal power with photovoltaic modules embedded in building façade [submitted/unpublished Ph.D. thesis]. Montréal, Québec, Canada: Department of Building, Civil and Environmental Engineering, Concordia University; August 2004
- [17] Dehra H. The effect of heat and thermal storage capacities of photovoltaic duct wall on co-generation of electric and thermal power. In: AIChE. 2007 Spring Meeting; April 22-26; Houston, Texas, USA. Session 36a. 2007. 9 p
- [18] Dehra H. The entropy matrix generated exergy model for a photovoltaic heat exchanger under critical operating conditions. *International Journal of Exergy*. 2008;**5**(2):132-149
- [19] Dehra H. A two dimensional thermal network model for a photovoltaic solar wall. *Solar Energy*. 2009;**83**(11):1933-1942
- [20] Dehra H. Electrical and thermal characteristics of a photovoltaic solar wall with passive and active ventilation through a room. *International Journal of Energy and Power Engineering*. 2017;**11**(5):514-522. <http://waset.org/publications/10007024>
- [21] Dehra H. An investigation on energy performance assessment of a photovoltaic solar wall under buoyancy-induced and fan-assisted ventilation system. *Applied Energy*. 2017;**191**(1):55-74
- [22] Dehra H. A combined solar photovoltaic distributed energy source appliance. *Natural Resources*. 2011;**2**:75-86
- [23] Dehra H. A mathematical model of a solar air thermosyphon integrated with building envelope. *International Journal of Thermal Sciences*. 2016;**102**:210-227

IntechOpen



# We are IntechOpen, the world's leading publisher of Open Access books Built by scientists, for scientists

6,300

Open access books available

171,000

International authors and editors

190M

Downloads

Our authors are among the

154

Countries delivered to

TOP 1%

most cited scientists

12.2%

Contributors from top 500 universities



WEB OF SCIENCE™

Selection of our books indexed in the Book Citation Index  
in Web of Science™ Core Collection (BKCI)

Interested in publishing with us?  
Contact [book.department@intechopen.com](mailto:book.department@intechopen.com)

Numbers displayed above are based on latest data collected.  
For more information visit [www.intechopen.com](http://www.intechopen.com)



---

# Conductive Copper Paste for Crystalline Silicon Solar Cells

---

Sang Hee Lee and Soo Hong Lee

Additional information is available at the end of the chapter

<http://dx.doi.org/10.5772/intechopen.78604>

---

## Abstract

In photovoltaic industries, the main technique of metallization is screen printing with silver pastes due to its simple and quick process. However, the expensive price of silver paste is one of the barriers to the production of low-cost solar cells. Therefore, the most focused target in photovoltaic research is the decreasing consumption of silver paste or substitute silver for other materials. As a proper candidate, copper has been researched by many institutes and companies since it has a similar conductivity with silver even though the price is inexpensive. To apply copper as a contact for solar cells, the plating technique has been actively researched. However, copper paste, which was mainly developed for integrated circuit applications, has been recently researched. Mostly, copper paste was developed for the low-temperature annealing process since copper tends to oxidize easily. On the other hand, firing type copper paste was also developed by coating copper particles with a barrier layer. This chapter discusses recent development of copper paste for the application of solar cells and its appropriate annealing conditions for better electrical properties. Also, the light I-V characteristics of copper paste on the solar cells in other research papers are summarized as well.

**Keywords:** copper paste, oxidation barrier coating, curing, silicon heterojunction solar cells, passivated busbar

---

## 1. Introduction

In photovoltaic industries, screen printing is the most dominant metallization technique for silicon-based solar cell fabrication as it is quick and simple. As a material of front contact, silver is the favorable metal since it has high conductivity [1] and is chemically inactive. However, screen printing with silver paste is the most expensive portion in cell production

---

after the silicon material cost [2]. Therefore, reducing the amount of silver consumption per cell or replacing silver to other metal materials is a significant research area.

According to the international technology roadmap for photovoltaic (ITRPV) published in 2016, silver consumption per cell will decrease until 40 mg/cell in 2026 with developments of pastes and screens, which is around 40% lower than now (95 mg/cell) [3]. On the other hand, substituting silver for copper has been actively researched since the cost of copper is cheaper than silver (approximately a 50 times) and has a similar conductivity (silver:  $1.6 \mu\Omega\text{-cm}$ , copper:  $1.7 \mu\Omega\text{-cm}$ ) [4, 5]. In order to share new information and go over the technical limitations, workshops for the metallization of crystalline silicon solar cells have been organized since the first workshop in Utrecht, Netherlands, in 2008 [6].

Researches concerning copper contact mainly have been carried out by the plating technique due to its various advantages, such as high aspect ratio and low contact resistance, which result in a high-efficiency solar cell over 21% [7–12]. Meanwhile, the application of screen-printable copper paste on solar cells has been studied as it can be easily applied to the established cell production line. In the case of the copper paste, copper particles cannot be deposited directly on the emitter, because the copper atoms have fast diffusion velocity and acts as a deep-level impurity in the crystalline silicon solar cell [13–18]. The copper atoms in the silicon produce generation and recombination centers and degrade the minority carrier lifetime of the crystalline silicon solar cells [11, 19–21]. Accordingly, most of the copper pastes on the solar cells were printed above the passivation layer as a busbar, which is called “passivated busbars”, while the silver paste fingers contacted the silicon. **Figure 1** shows the fingers and a busbar of the solar cell that are printed by silver paste. Similar to the finger, the role of the busbar on the solar cell is a collection of charge carriers generated by incident light in the absorb layer. The busbar is also connected to the soldered ribbon to extract carriers out of the device. To connect a busbar with a ribbon, the busbar should be printed with similar width of the ribbon which is usually 1.5 mm on the commercial type of solar cells. Accordingly, researchers have tried to apply copper paste only for the busbar since most of the silver paste usage is for the busbar, while the fingers were still printed by silver paste or deposited by the plating technique.

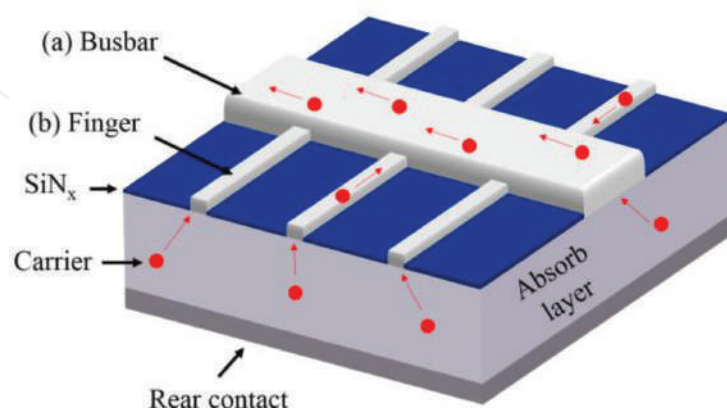


**Figure 1.** Carrier collection by the screen-printed silver (a) busbar and (b) finger [26].

Nonetheless, it is possible that the copper paste can be in direct contact with the silicon if the copper particles are coated with barrier layers in order to prevent copper from diffusing into the silicon. Another issue of copper in the application to the paste form is that copper tends to oxidize easily during thermal treatment [13, 22–25]. Since copper oxide shows an electrically nonconductive characteristic, it will increase the series resistance in the solar cells. Due to these reasons, copper paste has been continuously researched by several institutes and companies in order to overcome such issues. Section 2 deals with research trends of the copper paste components and promising coating techniques of copper powder for better reliability. Afterwards, Section 3 discusses appropriate curing conditions of polymer-based copper paste and the results of copper paste application to the silicon solar cells.

## 2. Copper paste developments for the crystalline silicon solar cells

In the 1990s, copper paste was researched for the application of integrated circuits, such as print circuit boards, because copper has a high electrical conductivity, a high thermal conductivity, excellent solderability, and a low electron migration [27–29]. With the increase in circuit density, properties of copper paste needed to be improved. The researched topics were mainly focused on optimizing the size of metal particles to enhance the density and printability of paste [30, 31]. Recently, copper paste has been developed for the application of the crystalline silicon solar cells as the low-cost front contact.

### 2.1. Structure of metallized solar cells with screen-printed pastes

Copper paste is generally compared to silver paste since it is a dominant material for the front metallization of the crystalline silicon solar cell. In order to apply copper paste to the solar cells, the properties of copper paste, such as printability and solderability, need to have similar or better characteristics than silver paste. Electronic pastes are generally composed of conductor metal (Ag, Au, Pd, Cu, etc.), glass frits, and organic vehicle [32, 33]. One of the important components of the conventional silver paste for the front contact of the crystalline silicon solar cell is glass frits. In case of the crystalline silicon solar cells based on the silver paste, the dielectric layer, which is usually silicon nitride ( $\text{SiN}_x$ ), is fired-through above  $600^\circ\text{C}$  and the silver particles contact the emitter (**Figure 2(a)**).

On the other hand, if the copper paste has the same process as the silver paste, the diffused copper can adversely effect on the characteristics of the solar cell as we mentioned earlier. Thus, for applying copper paste to the crystalline silicon solar cell, copper particles in the paste need to be coated by barrier layers. In this case, the copper paste can be fired at a similar temperature range as the silver paste and contact the emitter (**Figure 2(b)**). Otherwise, the contact should be formed without penetrating the  $\text{SiN}_x$  layer (**Figure 2(c)**) by applying the curing type copper paste which does not need the glass-frits components for the fired-through contact.

Silicon heterojunction (SHJ) solar cells have typically a low process temperature limit ( $\sim 250^\circ\text{C}$ ) because high-temperature annealing processes can degrade the passivation of the

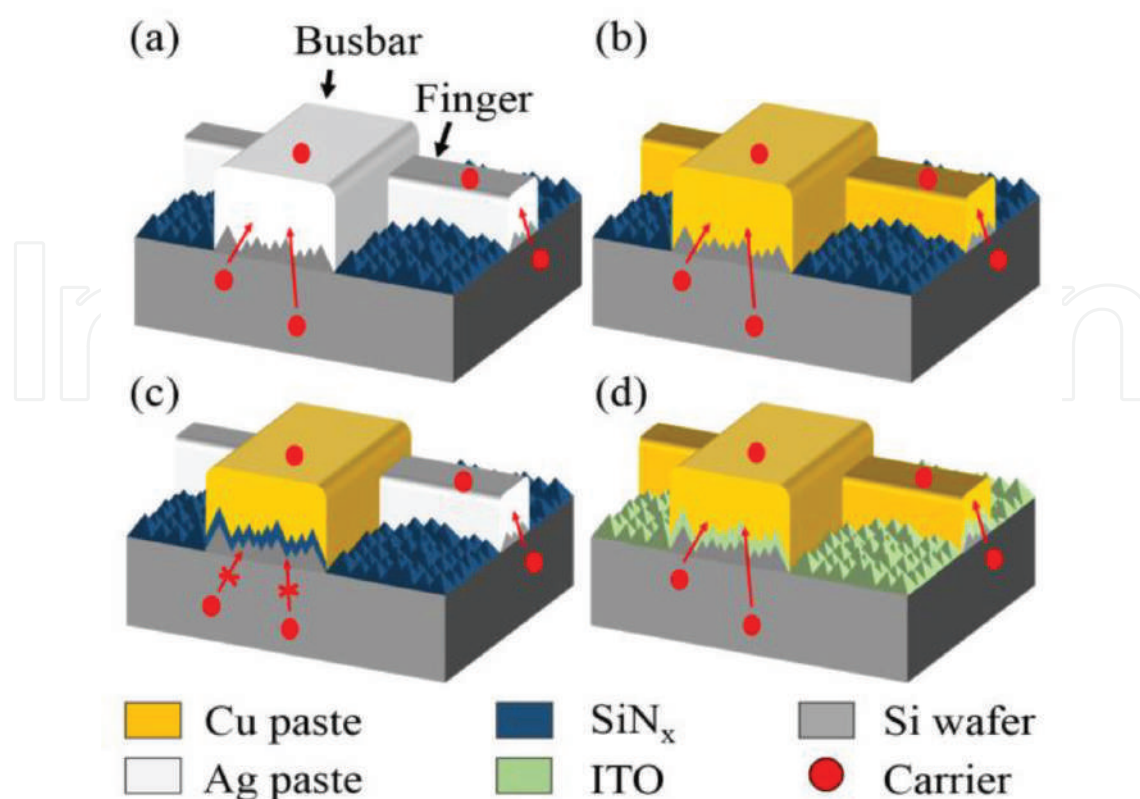


**Figure 2.** (a) Conventional silicon solar cell contact with silver paste, (b) contact with firing-type copper paste, (c) contact with curing-type copper paste, and (d) contact with curing-type copper paste on the SHJ solar cell [26].

hydrogenated amorphous silicon (a-Si:H) due to the hydrogen effusion during the annealing [34]. For this reason, the curing-type copper paste, where low temperature is generally required, is beneficial to the SHJ solar cells. Also, if copper paste is printed on the indium tin oxide (ITO) layer of the SHJ solar cell (**Figure 2(d)**), ITO can act as a diffusion barrier for preventing copper diffusion [35]. The next section discusses detail components of the copper pastes for the application of the solar cells by categorizing the annealing temperature of the paste.

## 2.2. Copper paste for high-temperature annealing (firing type)

In 2011, a copper paste that is chemically and metallurgically similar to conventional silver paste was developed by Applied Materials, Inc. [36]. The copper paste can be fired through a  $\text{SiN}_x$  layer and the metal particles directly contact silicon (**Figure 2(b)**). The main components and possible materials of the invented copper paste are listed in **Table 1**. The invented technique involves copper-containing particles being encapsulated by additional layers of metal and alloys to restrict oxidation and diffusion of copper during the firing. For improving the oxidation resistance of copper, alloying copper with other metals (Ti, Mg, Al, Pd, Ag, Ni, Cr, and Zr) has been researched [37–40]. The Cu-Ag alloy is estimated as the best materials for improving oxidation resistance with only a slight reduction in electrical conductivity [41]. The paste of this group also uses doped copper or copper alloys rather than pure copper particles,

Components	Materials	Purposes
Metal powder	Doped copper (aluminum, magnesium, etc.), copper alloys (CuSn, CuAg, CuNi, CuZn, etc.)	To have conductive property
Polymer resin	Ethylcellulose	To enable printing of copper-containing particles
Glass frits	Lead oxide (PbO <sub>x</sub> ), silicon oxide (SiO <sub>2</sub> ), alumina (Al <sub>2</sub> O <sub>3</sub> ), boron trioxide (B <sub>2</sub> O <sub>3</sub> ), zirconia (ZrO <sub>2</sub> ), zinc oxide (ZnO), bismuth oxide (Bi <sub>2</sub> O <sub>3</sub> ), strontium oxide (SrO), titanium oxide (TiO <sub>2</sub> ), and lanthanum oxide (La <sub>2</sub> O <sub>3</sub> )	To pass through a passivation layer and promotes adhesion to the substrate
Solvents	$\alpha$ -Terpineol, toluene, ethanol	To tune viscosity characteristics

**Table 1.** Components and possible materials of the copper paste for high-temperature annealing.

because alloying elements in copper reduce the contact with oxygen. Generally, the polymer resin acts as a binder to enable printing of the encapsulated copper-containing particles and is typically removed during the firing by oxidation.

**Figure 3** shows three levels of encapsulation for preventing copper particles from oxidation and diffusion. Simply, the copper-containing particle can be coated by oxidation barrier layers. Also, a metallization barrier layer can be used under the oxidation barrier since the oxidation layer can form an alloy with the inside material. Moreover, a diffusion barrier can directly surround the copper-containing particle for a more perfect encapsulation. The possible materials for the encapsulation layer are listed in **Table 2**.

### 2.3. Copper paste for low-temperature annealing (curing type)

In order to create a solderable surface on the ITO of the SHJ solar cells, polymer-based silver pastes were commonly used in the solar cell industry, because silver has a low contact resistivity on ITO and low line resistances. However, reactions between polymer and solder flux during the annealing result in a “solder leaching” problem. If the screen-printed paste is dissolved in the solder material due to the solder leaching, it leads to low adhesion and high contact resistivity between paste and solder material.

Using copper instead of silver, as a metal powder in the polymer-based paste, is a good solution in order to overcome the issue of solderability, because copper produces a comparable solderability and resistance at a much lower price [42]. For these reasons, polymer-based copper paste for low-temperature annealing has been researched as a promising product in the future with the fact that the SHJ solar cells have become common in the PV industry [43–46]. From now on, the components and properties of the curing-type copper pastes from some groups will be discussed.

#### 2.3.1. Dow Corning

Dow Corning reported papers and patents about a curing-type copper paste and the applicable solar cell structures [47–51]. The curing is referred to as the hardening of polymer materials

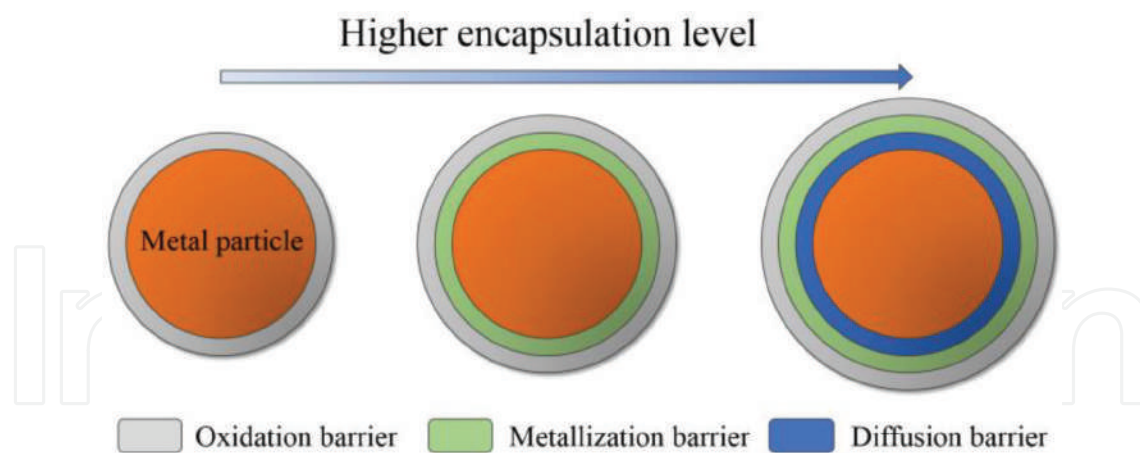


**Figure 3.** Cross-sectional views of encapsulated copper-containing particles with single and multi-barrier layer.

Encapsulation layer	Oxidation barrier	Metallization barrier	Diffusion barrier
Possible materials	Silver (Ag), nickel (Ni), and zinc (Zn)	Nickel (Ni), titanium (Ti), titanium nitride (TiN), tungsten (W), titanium-tungsten (TiW), cobalt (Co), tungsten doped cobalt (Co:W), molybdenum (Mo), tantalum (Ta), and chromium (Cr)	

**Table 2.** The possible materials of each encapsulation layer for copper-containing particles.

by cross-linking polymer chains that can be processed by heating at a low temperature under 300°C. The copper paste consists of metal powder, solder powder (lower melting temperature than that of the metal powder), a polymer, a solvent, a cross-linking agent, and additives. The solder powder comprises at least one of a tin-bismuth (SnBi) alloy, a tin-silver (SnAg) alloy, or combinations of them. The polymer and the carboxylated polymer are made of an epoxy resin and an acrylic polymer, respectively. The cross-linking agent (or catalyst) can be chosen from carboxylated polymers, dimer fatty acids, and trimer fatty acids. Among the dimer fatty acid, dicarboxylic acid and monocarboxylic acid are useful for fluxing the metal powder and cross-linking the polymer. Moreover, a solvent and an adhesion promoter can be included as additive components.

This copper paste is used to form a busbar of the conventional crystalline silicon solar cell without a fired-through process. **Figure 4** shows that the printed busbar has a brown-red color due to the copper particles. Afterwards, the color of the busbar changes to gray after the curing process because the copper particles are coated by the solder. The cells with the copper busbar have a higher front surface minority carrier lifetime than the cells with the silver fired-through busbar since the covered area under the busbar is fully passivated. The detail characteristics will be mentioned in Section 3.

### 2.3.2. National Institute of Advanced Industrial and Scientific Technology (AIST)

A research group in the AIST also reported a similar concept of the copper paste as the Dow Corning's copper paste. Their copper paste, which is called "copper-alloy paste," is composed

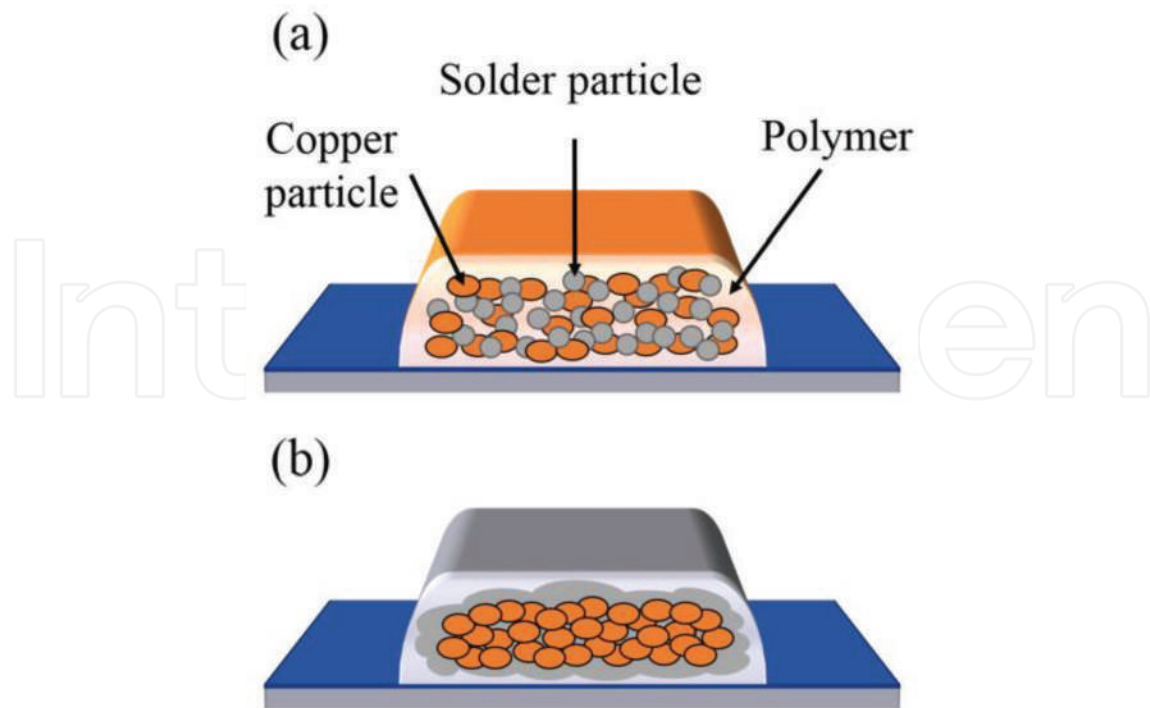


**Figure 4.** Dow Corning's screen-printable copper paste: (a) after printing and (b) after curing [26].

of conductive metal particles, low melting point alloy (LMPA), thermosetting polymer, and solvent [52]. During the curing process, the molten LMPA particles form alloy with the copper particles and surround the copper particles to prevent oxidation. In particular, the LMPA allows the curing process to set the temperature below 200°C without any reductive conditions unlike the conventional silver paste. The result of the differential scanning calorimetry (DSC) shows that the melting point of the LMPA is 143°C. The peak of the DSC graph is very sharp since the LMPA had a nano-level uniformity. Moreover, the copper-alloy paste shows better self-leveling and resolution than the conventional silver paste after the screen-printing process on a textured silicon wafer.

Also, the copper paste from this group shows decent reliability after printing as a busbar on p-type crystalline silicon [53]. The samples were tested by the damp heat test (DHT) and thermal cycling test (TCT) before and after the encapsulation with the "sandwich" structure (glass/EVA/cell/EVA/backsheet) according to the IEC61215 standards. The results of both DHT and TCT show degradation less than 5% of the initial values in all parameters ( $V_{oc}$ ,  $J_{sc}$ , FF,  $P_{max}$ , etc.) before and after encapsulation. Although the surface of the copper electrode without encapsulation is oxidized after the DHT test, the copper oxide layer acts as a semi-passivation layer that postpones inner oxidation. Moreover, the copper particles in their paste do not diffuse into the silicon even after an hour of annealing at 400°C due to the polymer barrier layer.

### 2.3.3. Samsung Electro-Mechanics Co., Ltd.

The invented copper paste was focused on the nano-particle size copper powder, especially for substrates (such as a transparent conductive oxide (TCO), a polymer, a glass plate, and a printed circuit board), which have difficulties in applying high-temperature processes [54, 55].

The average particle size of copper is around 150 nm, and the surfaces of the copper particles are coated with a capping material which can be fatty acid or fatty amine. The nano-size copper powder is used either solely as a metal powder or with different sizes of copper particles, such as a flake powder and a spherical powder. The flake powder has a particle size of 1–20  $\mu\text{m}$  and the spherical powder has a 0.1–5- $\mu\text{m}$  particle size. When the nano-powder is mixed with other types of powder, it first dissolves during the annealing and then helps to connect between the larger copper particles. Because of this nano-size effect, this copper paste can enhance conductivity. The detailed candidates for binders and additives are also presented in the patent. Consequently, the copper particle at 150-nm size decreases the annealing temperature of the paste and makes it possible to form electrodes at a low temperature of 200°C.

#### 2.3.4. Institute of Nuclear Energy Research (INER)

Recently, the INER reported an antioxidant copper paste [56, 57]. The antioxidant copper nanoparticles are synthesized by a wet chemical reduction process which requires copper hydroxide ( $\text{Cu}(\text{OH})_2$ ), polyvinylpyrrolidone (PVP), and ascorbic acid. Afterwards, the antioxidant copper nanoparticles are transferred to the paste form and printed onto the ITO layer of SHJ solar cells, followed by low-temperature annealing (<300°C). Compared to commercial silver pastes as a reference, this copper paste shows a twofold increase in sheet resistance ( $\sim 30 \text{ m}\Omega/\text{sq}$ ) on the 16  $\mu\text{m}$  of printed films. However, the duration of copper paste annealing is 1/12 of that of silver paste. Also, reserving samples for 180 days without strict oxygen protection shows no peaks of oxide impurities after XRD characterization, which means that the copper film is relatively stable against oxidation at least at an X-ray detection level.

### 2.4. Promising techniques for high performance of copper paste

#### 2.4.1. Coating of copper powder with nano-silica

In order to apply copper on conductive paste, it requires high-purity crystalline non-agglomerated copper powder, which is free from surface oxidation [58, 59]. Using silica as a coating material of copper powder can enhance colloidal properties and functions by using rational core-shell shapes [60]. Dong et al. coated nano-copper powder with nano-silica by using a sol-gel process to improve the dispersion of the glass in the paste, the density of films, and the bonding behavior between the film and the substrate [61]. The printed films by using the copper paste after sintering at 910°C show no significant change in the density of the surface morphology and sheet resistance with the contents of silica from 0.5 to 2 wt%. However, the bonding between the film and the substrate improves with 2 wt% of silica contents in copper powder. The reason is that the proper amount of silica contents can induce the capillary effects and surface sorption effects which is beneficial to bond the film closely on the substrate. The properties of silica-coated copper powder will be able to improve the bonding of the high-temperature annealing copper paste on the silicon wafers.

#### 2.4.2. Coating of copper powder with cobalt-catalyzed carbon nanofibers

Even though the properties of polymer-based copper paste have been improved by many research, it is still difficult to achieve high conductivity and reliability as silver paste due to

the relatively low conductivity of the polymers [62–66]. In addition, using nanoscale copper particles for decreasing curing temperature also have issues of powder production step, such as controlling the size of particles [67], low oxidation resistance of particles [68, 69], and cost-effectiveness [70]. For this reason, the development of copper particles, which are coated by a carbon-based material, has been interested by many researchers, because carbon shells can act as the shields to protect the copper particles from oxidation [71–79]. In addition, there have been studies for the development of copper paste or ink, which do not require inert atmosphere and lower temperature, but they still have challenges to overcome [80–83].

In order to improve oxidation resistance of copper particles and make curing process possible in air, Ohnishi et al. coated copper-cobalt alloy particles with cobalt-catalyzed carbon nanofibers (CNFs) which is called “hybrid copper particles (HCuP)” [84]. The paste, which is made by the sea urchin-shaped copper particles, shows great reliability of resistivity even after a DHT test. The good electrical properties of this copper paste might come from an anti-oxidation effect of CNFs. Moreover, the cobalt nano-precipitates on the surface of the particles can be regarded as a conductive path. This approach possibly can improve the reliability of copper pastes by curing without strictly controlled inert atmosphere.

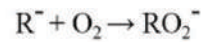
### 3. Application of copper paste on crystalline silicon solar cells

#### 3.1. Curing conditions of copper paste for high electrical properties

Low-temperature annealing paste generally contains polymer as a component. Accordingly, the properties of these pastes highly depend on the polymerization quality during the curing process. The curing process is carried out at a lower-temperature range than the firing process, which is generally used for the conventional silver paste. *Rehm thermal systems GmbH* and *Fraunhofer Institute for Ceramic Technologies and Systems* reported the effect of curing conditions on properties of the electrode which is printed with the polymer-based copper paste [22, 42, 62, 85]. By using an inert inline drying system, they show that curing with a high nitrogen atmosphere and temperature at 200°C can significantly decrease the resistance of copper paste electrode [42].

The main reason of the resistance reduction is that the cross-linking reactions of polymer chains are sensitive to the oxygen concentration, because the oxygen disturbs the linking process between the polymer chains. **Figure 5** shows the reactions of degradation of the polymer chain which frequently occurs in a high oxygen atmosphere. Oxygen easily reacts with most organic radicals which form “peroxidic radicals” [86]. The peroxidic radicals can suffer the polymerization reactions or the chain processes. As one of the most frequent reactions, an oxidative degradation breaks the polymer chains by initiating the decomposition of the peroxidic radicals. If the polymerization process is carried out in this circumstance, oxygen presence will decrease the cross-linking yield of polymers in the pastes. Therefore, the inert curing atmosphere with low concentration of the oxygen is significant in order to make an intensified polymerization and increase the compression of the metal particles. The restrained oxidation of the metal particles can also be a possible reason.

*Reaction 1: peroxidic radicals formation*



*Reaction 2: decomposition of polymer chain*

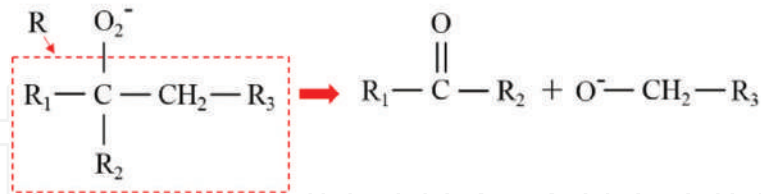


**Figure 5.** Reactions of polymer chain decomposition by oxygen.

In case of the heat transfer method, a radiation method is more beneficial for the lower resistance of electrode than a convection method [62]. Moreover, the minimum resistance and decent adhesion can be obtained by increasing the processing time [22]. Consequently, this group confirmed that the polymer-based copper paste, which was annealed by the inert curing, can improve conductivity and mechanical stability of the polymer-based copper paste by achieving 19.96% efficiency with the SHJ solar cell, even though the fill factor (FF) is still lower than that of silver paste-printed cells.

### 3.2. Potential of copper paste on the silicon solar cells as passivated busbars

Some research groups have tried to apply their own copper paste to solar cells. The copper pastes were printed as passivated busbars that required forming busbars and fingers separately. As **Figure 4** shows, fingers only electrically contact silicon by using either fired-through silver paste (**Figure 6(b)**) or the plating of Ni/Cu/Ag metal stack after the laser ablation opening of  $SiN_x$  layer (**Figure 6(a)**). Afterwards, the busbar is printed on the  $SiN_x$  layer and partially contacts the fingers followed by a curing process under  $250^\circ C$ . Since the busbars do not directly contact the silicon, recombination region under the busbars is removed. Light I-V performances of the solar cells with copper paste busbar are summarized in **Table 3**. On the reference cells, either the screen-printed silver paste contact or the Ni/Cu/Ag-plated contact was wholly used for the busbars and fingers. Generally, the reduced recombination on the front side contributes to an increase open circuit voltage ( $V_{oc}$ ) compared to the cells without passivated busbar.

Dow Corning and IMEC evaluated characteristics of various cell structures by applying their own low-temperature ( $\sim 250^\circ C$ ) copper paste for the passivated busbars. The research results show a slight increase of  $V_{oc}$  (0.3 mV) with an industrial level passivated emitter solar cell (PESC) by reducing the recombination region under the busbars. Compared to the conventional silver paste solar cell, the passivated copper busbar solar cell has a lower average fill factor (FF) due to the higher lateral resistivity of the copper busbar. However, the busbar resistivity does not have an effect on the FF in the module level performance since most of lateral current flows through the conductive soldered tab.

This group also evaluated combinations of printable conductive copper paste with higher efficiency solar cell structures, such as passivated emitter and rear cell (PERC) and passivated

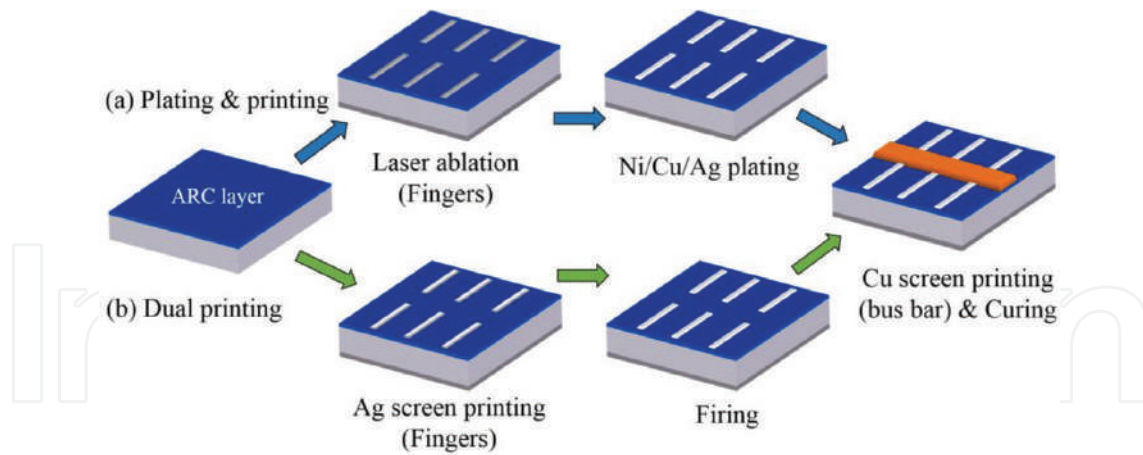


**Figure 6.** Front metallization process flows for the passivated copper busbar: (a) plating and printing, and (b) dual printing [26].

Institute	Year	Cell type	Ref. contact	$\eta$ [%] (gain)	$V_{oc}$ [mV] (gain)	$J_{sc}$ [mA/ cm <sup>2</sup> ]	FF [%] (gain)	Annealing temp.	Ref.
Dow Corning	2014	p-PESC (SE)	SP*-Ag	18.8 (-0.07)	640.4 (+0.3)	37.2	78.9 (-0.5)	~250°C	[47]
Dow Corning	2015	p-PERC	Plated-Ni/ Cu/Ag	20.4 (+0.1)	667.5 (+6.1)	38.7	79.0 (+0.3)	~250°C	[48]
Dow Corning	2015	n-PERT	Plated-Ni/ Cu/Ag	20.7 (0)	663.3 (+4.9)	39.2	79.5 (0)	~250°C	[48]
Meiji Univ.	2015	n-PERT (bifacial)	SP-Ag	20.5 (+0.7)	659.0 (+3.0)	40.8	76.3 (+2.0)	—	[87]
Tokyo Univ.	2012	p-PESC (mc-Si)	SP-Ag	16.2 (+0.1)	617.0 (-2.0)	34.3	76.3 (+0.1)	<200°C	[88]

\*SP: screen printed.

**Table 3.** Performance of various solar cell structures with the passivated copper busbar and gains compared to their reference contact.

emitter and rear totally diffused (PERT). By applying a copper paste busbar with the plating and printing process as depicted in **Figure 6(a)**, both structures improved 6.1 mV, 4.9 mV of  $V_{oc}$ , respectively, and the PERC structure especially had a 0.1% higher median conversion efficiency than the reference group. Also, the FF of the passivated busbar cells had increased since the laser ablation and the nickel silicide decreased the shunt resistance of entirely plated cells. In the case of the current density, the passivated busbar cell had a slightly lower value even though the series resistance of both the printed busbar and the plated busbar almost had no difference since the plated busbar had a higher aspect ratio (fine line width).

Nakamura et al. at the Meiji University applied copper paste on the n-type bifacial PERT cell and successfully obtained over 20% efficiency by preceding  $V_{oc}$  and FF of the silver-printed cell. Also, Yoshiba et al. at the Tokyo University compared the I-V performances on the

multi-crystalline silicon solar cell by printing a low melting point alloy (LMPA) copper paste. Although  $V_{oc}$  was decreased, copper-printed cell had a 0.1% absolute efficiency gain due to the higher FF. In most of the experiments for confirming applicability of copper paste on solar cell fabrication, the results show the possibility of reduction of metallization cost and cell performance improvement by replacing the standard silver-printed electrode.

#### 4. Summary and outlook

In this chapter, a detailed overview of the copper paste developments for the solar cell application has been presented. The main issues of developing copper paste are prohibition of the oxidation of copper during annealing and the diffusion into the silicon substrate. In case of the glass-frit-based copper paste (firing type), the copper particles are coated with metal or alloy layers to prevent the diffusion and the oxidation. However, the firing-type copper paste still has a higher possibility of diffusion than the polymer-based copper paste (curing type) since the copper particle comes in direct contact with the silicon. In case of the curing-type copper paste, the diffusion of copper particles is well blocked since the surrounding polymer acted as a barrier layer. Also, the oxidation of copper can be prevented by the polymer shield or using antioxidant copper particles. Moreover, DHT and TCT of the copper paste confirm the reliability on the solar cells with a small amount of degradation (<5%).

For further improvement of the copper paste properties, recently reported coating materials and techniques for the copper powder have been introduced. In case of the nano-silica coating on copper powder, the bonding strength of paste on the substrate was improved by promoting capillary effects and surface sorption effects. Also, the air-curable hybrid copper particles, which were coated by cobalt-catalyzed-CNFs, lead to a great resistance reliability of the printed copper paste.

With respect to the curing conditions, the experimental results revealed that the inert atmosphere helps to form a denser copper electrode by restricting the contact between the polymers and the oxygen. Thereby, the compressed copper particles due to the intensified polymerization decrease the resistivity of the printed copper film. However, the inert curing condition requires a great deal of nitrogen gas for purging oxygen in the furnace. At the industrial level, the nitrogen consumption can adversely affect the manufacturing cost of the solar cells. Therefore, the optimum curing process for less consumption of nitrogen gas and inexpensive coating technique of copper particles need to be further developed.

To date, polymer-based copper paste showed a high potential with 20.7% conversion efficiency by applying it to the n-PERT structure solar cells. As well as the result of the PERT structure, the copper paste application to SHJ solar cells has a higher potential because the ITO layer acts as a diffusion barrier to prevent copper at a low curing temperature. Also, the use of copper paste, as the passivated busbars, requires an additional printing, and the annealing step after the silver fingers and aluminum rear contact are formed. Accordingly, the SHJ solar cells are more profitable for the application of copper paste from an economic point of view.

## Acknowledgements

This work was supported by the Korea Institute of Energy Technology Evaluation and Planning (KETEP) and the Ministry of Trade, Industry & Energy (MOTIE) of the Republic of Korea (No. 20173010012940) and by the Ministry of Trade, Industry, and Energy, Korea Evaluation Institute of Industrial Technology (KEIT) (No. 10043793).

## Author details

Sang Hee Lee and Soo Hong Lee\*

\*Address all correspondence to: [shl@sejong.ac.kr](mailto:shl@sejong.ac.kr)

Department of Electronics Engineering, Green Strategic Energy Research Institute, Sejong University, Seoul, Korea

## References

- [1] Park K, Seo D, Lee J. Conductivity of silver paste prepared from nanoparticles. *Colloids and Surfaces A: Physicochemical and Engineering Aspects*. 2008;**313**:351-354
- [2] Powell DM, Fu R, Horowitz K, Basore PA, Woodhouse M, Buonassisi T. The capital intensity of photovoltaics manufacturing: Barrier to scale and opportunity for innovation. *Energy & Environmental Science*. 2015;**8**:3395-3408
- [3] International Technology Roadmap for Photovoltaic (ITRPV). Available from: <http://www.itrpv.net> [Accessed: 2016-Mar]
- [4] London Bullion Market Association (LBMA). Available from: <http://www.lbma.org.uk/home> [Accessed: 2017-Mar]
- [5] London Metal Exchange. Available from: <https://www.lme.com/metals/non-ferrous/nickel> [Accessed: 2017-Mar]
- [6] Workshop on Metallization for Crystalline Silicon Solar Cells. Available from: <http://www.metallizationworkshop.info>
- [7] Horzel J, Bay N, Passig M, Sieber M, Burschik J, Kühnlein H, Brand A, Letize A, Lee B, Weber D, Böhme R. Low cost metallization based on Ni/Cu plating enabling high efficiency industrial solar cell. In: *Proceeding of the 29th European Photovoltaic Solar Energy Conference and Exhibition; 2014; Amsterdam, Netherland*. pp. 507-512
- [8] Bay N, Horzel J, Passig M, Sieber M, Burschik J, Kühnlein H, Bartsch J, Brand A, Mondon A, Eberlein D, Völker C, Gutscher S, Letize A, Lee B, Weber D, Böhme R. Reliable contact formation for industrial solar cell by laser ablation and Ni/Cu plating. In: *Proceedings*

of the 29th European Photovoltaic Solar Energy Conference and Exhibition; 2014; Amsterdam, Netherland. pp. 1272-1276

- [9] Hernández JL, Adachi D, Yoshikawa K, Schroos D, Assche EV, Feltrin A, Valckx N, Menou N, Poortmans J, Yoshimi M, Uto T, Uzu H, Hino M, Kawasaki H, Kanematsu M, Nakano K, Mishima R, Kuchiyama T, Koizumi G, Allebé C, Terashita T, Hiraishi M, Nakanishi N, Yamamoto K. High efficiency copper electroplated heterojunction solar cells. In: Proceedings of the 27th European Photovoltaic Solar Energy Conference and Exhibition; 2012; Frankfurt, Germany. pp. 655-656
- [10] Papet P, Hermans J, Söderström T, Cucinelli M, Andreetta L, Bätzner D, Frammelsberger W, Lachenal D, Meixenberger J, Legradic B, Strahm B, Wahli G, Brok W, Geissbühler J, Tomasi A, Ballif C, Vetter E, Leu S. Heterojunction solar cell with electroplated Ni/Cu front electrode. In: Proceedings of the 28th European Photovoltaic Solar Energy Conference; 2013; Paris, France. pp. 1976-1979
- [11] Bartsch J, Mondon A, Kamp M, Kraft A, Wendling M, Mehling M, Wehkamp N, Jawaïd M, Lorenz A, Clement F. Copper as conducting layer in the front side metallization of crystalline silicon solar cells—Challenges, processes and characterization. Proceedings of the 2nd Workshop on Metallization for Crystalline Silicon Solar Cells—Status, Trends and New Directions, Constance, Germany, Konstanz, Germany; 2010. pp. 32-37
- [12] Metz A, Adler D, Bagus S, Blanke H, Bothar M, Brouwer E, Dauwe S, Dressler K, Droessler R, Droste T. Industrial high performance crystalline silicon solar cells and modules based on rear surface passivation technology. *Solar Energy Materials and Solar Cells*. 2014;**120**:417-425
- [13] Istratov AA, Weber ER. Physics of copper in silicon. *Journal of The Electrochemical Society*. 2002;**149**:G21-G30
- [14] Brotherton S, Ayres J, Gill A, Van Kesteren H, Greidanus F. Deep levels of copper in silicon. *Journal of Applied Physics*. 1987;**62**:1826-1832
- [15] Kaimao C, Zhongan W. Deep levels related to copper in silicon. *Journal of Electronics (China)*. 1988;**5**:285-293
- [16] Aboelfotoh M, Svensson B. Copper passivation of boron in silicon and boron reactivation kinetics. *Physical Review B*. 1991;**44**:12742
- [17] Murarka SP, Hymes SW. Copper metallization for ULSL and beyond. *Critical Reviews in Solid State and Materials Sciences*. 1995;**20**:87-124
- [18] Murarka SP. Advanced materials for future interconnections of the future need and strategy: Invited lecture. *Microelectronic Engineering*. 1997;**37**:29-37
- [19] Schibli E, Milnes A. Deep impurities in silicon. *Materials Science and Engineering*. 1967;**2**:173-180
- [20] Weber ER. Transition metals in silicon. *Applied Physics A: Materials Science & Processing*. 1983;**30**:1-22

- [21] Ur Rehman A, Lee SH. Crystalline silicon solar cells with nickel/copper contacts. In: *Solar Cells—New Approaches and Reviews*. InTech; 2015
- [22] Clement C, Bell H, Vogg F, Rebenklau L, Gierth P, Partsch U. Inert drying system for copper paste application in PV. *Energy Procedia*. 2013;**38**:423-429
- [23] Mimura K, Lim J-W, Isshiki M, Zhu Y, Jiang Q. Brief review of oxidation kinetics of copper at 350 C to 1050 C. *Metallurgical and Materials Transactions A*. 2006;**37**:1231-1237
- [24] Xu X, Luo X, Zhuang H, Li W, Zhang B. Electroless silver coating on fine copper powder and its effects on oxidation resistance. *Materials Letters*. 2003;**57**:3987-3991
- [25] Jeong S, Woo K, Kim D, Lim S, Kim JS, Shin H, Xia Y, Moon J. Controlling the thickness of the surface oxide layer on cu nanoparticles for the fabrication of conductive structures by ink-jet printing. *Advanced Functional Materials*. 2008;**18**:679-686
- [26] Lee SH, Lee DW, Lee SH. Review of conductive copper paste for c-Si solar cells. *Korean Journal of Metals and Materials*. 2017;**55**:637-644
- [27] Wu S. Preparation of ultra-fine copper powder and its lead-free conductive thick film. *Materials Letters*. 2007;**61**:3526-3530
- [28] Huang C-Y, Sheen SR. Synthesis of nanocrystalline and monodispersed copper particles of uniform spherical shape. *Materials Letters*. 1997;**30**:357-361
- [29] Sinha A, Das SK, Kumar TV, Rao V, Ramachandrarao P. Synthesis of nanosized copper powder by an aqueous route. *Journal of Materials Synthesis and Processing*. 1999;**7**:373-377
- [30] Ogawa T, Asai T, Itoh O, Hasegawa M, Ikegami A, Atoh K, Kobayashi T. New thick-film copper paste for ultra-fine-line circuits. *IEEE Transactions on Components, Hybrids, and Manufacturing Technology*. 1989;**12**:397-401
- [31] Taylor BE, Tsuchiya M, Okabe C. Thick Film Copper Paste Composition. Google Patents; 1992
- [32] Brown O, Sridharan S. Lead-free and Cadmium-free Conductive Copper Thick Film Pastes. Google Patents; 2004
- [33] Brown O, Sridharan S. Lead-free and Cadmium-free Conductive Copper Thick Film Pastes. Google Patents; 2006
- [34] De Wolf S, Kondo M. Boron-doped a-Si: H/ c-Si interface passivation: Degradation mechanism. *Applied Physics Letters*. 2007;**91**:112109
- [35] Liu C, Liu W, Chen W, Hsieh S, Tsai T, Yang L. ITO as a diffusion barrier between Si and cu. *Journal of the Electrochemical Society*. 2005;**152**:G234-G239
- [36] Gee JM. Cu Paste Metallization for Silicon Solar Cells. Google Patents; 2011
- [37] Li J, Li Y, Wang Z, Bian H, Hou Y, Wang F, Xu G, Liu B, Liu Y. Ultrahigh oxidation resistance and high electrical conductivity in copper-silver powder. *Scientific Reports*. 2016;**6**:39650

- [38] Li J, Mayer J, Colgan E. Oxidation and protection in copper and copper alloy thin films. *Journal of Applied Physics*. 1991;**70**:2820-2827
- [39] Kawamura G, Alvarez S, Stewart IE, Catenacci M, Chen Z, Ha Y-C. Production of oxidation-resistant Cu-based nanoparticles by wire explosion. *Scientific Reports*. 2015;**5**:18333
- [40] An BW, Gwak E-J, Kim K, Kim Y-C, Jang J, Kim J-Y, Park J-U. Stretchable, transparent electrodes as wearable heaters using nanotrough networks of metallic glasses with superior mechanical properties and thermal stability. *Nano Letters*. 2015;**16**:471-478
- [41] Kim KO, Kim S. Surface morphology control of Cu-Ag alloy thin film on W diffusion barrier by seedless electrodeposition. *Journal of Nanoscience and Nanotechnology*. 2016;**16**:11701-11706
- [42] Rebenklau L, Gieth P, Partsch U, Mehlich H, Hausmann J, Grimm M, Stein W, Bell H, Clement C, Vogg F. Low temperature interconnection techniques for high efficiency heterojunction solar cells. In: *Proceeding of the 27th European Photovoltaic Solar Energy Conference*; 2012
- [43] Heng JB, Fu J, Kong B, Chae Y, Wang W, Xie Z, Reddy A, Lam K, Beitel C, Liao C. > 23% high-efficiency tunnel oxide junction bifacial solar cell with electroplated Cu gridlines. *IEEE Journal of Photovoltaics*. 2015;**5**:82-86
- [44] Kleider J-P, Alvarez J, Brézard-Oudot A, Gueunier-Farret M-E, Maslova O. Revisiting the theory and usage of junction capacitance: Application to high efficiency amorphous/crystalline silicon heterojunction solar cells. *Solar Energy Materials and Solar Cells*. 2015;**135**:8-16
- [45] Mishima T, Taguchi M, Sakata H, Maruyama E. Development status of high-efficiency HIT solar cells. *Solar Energy Materials and Solar Cells*. 2011;**95**:18-21
- [46] Wang Q, Page M, Iwaniczko E, Xu Y, Roybal L, Bauer R, To B, Yuan H-C, Duda A, Hasoon F. Efficient heterojunction solar cells on p-type crystal silicon wafers. *Applied Physics Letters*. 2010;**96**:013507
- [47] Wood D, Kuzma-Filipek I, Russell R, Duerinckx F, Powell N, Zambova A, Chislea B, Chevalier P, Boulord C, Beucher A. Passivated busbars from screen-printed low-temperature copper paste. *Energy Procedia*. 2014;**55**:724-732
- [48] Wood D, Kuzma-Filipek I, Russell R, Duerinckx F, Powell N, Zambova A, Chislea B, Chevalier P, Boulord C, Beucher A. Non-contacting busbars for advanced cell structures using low temperature copper paste. *Energy Procedia*. 2015;**67**:101-107
- [49] Boulord C, Chevalier PM, Powell NE, Zambova AP. Composition and conductor formed therefrom. *Google Patents*; 2012
- [50] Albaugh JD, Beaucarne GDS, Powell NE, Zambova AP. Photovoltaic cell and method of forming the same. *Google Patents*; 2012
- [51] Beaucarne GDS, Powell NE, Tous L, Wood DA, Zambova AP. Photovoltaic cell and method of forming the same. *Google Patents*; 2012

- [52] Yoshida M, Tokuhisa H, Itoh U, Kamata T, Sumita I, Sekine S. Novel low-temperature-sintering type cu-alloy pastes for silicon solar cells. *Energy Procedia*. 2012;**21**:66-74
- [53] Tokuhisa H, Ise S, Morita S, Tsukamoto S, Tomita M, Yoshida M. Reliability of a printed cu busbar electrode on a conventional silicon solar cell. *Japanese Journal of Applied Physics*. 2015;**54**:08KD22
- [54] Kim DH, Oh SI, Kang SK, Jun BH, Song YA, Kim SJ, Chun BJ. Copper nano paste, method for forming the copper nano paste, and method for forming electrode using the copper nano paste. Google Patents; 2011
- [55] Lee YI, Kim DH, Kim JY, Kwon JH, Kim SE. Conductive paste composition for low temperature firing. Google Patents; 2013
- [56] Chang W-C, Weng L-W, Chuang C-K, Liang J-X, Yang T-N, Ma W-Y. The preparation of antioxidant copper paste and its application to silicon solar cells. *Journal of Nanoscience and Nanotechnology*. 2016;**16**:9125-9131
- [57] Ma W-Y, Chang W-C, Weng L-W, Liang J-X, Chung C-H, Yang T-N. The preparation of antioxidative copper pastes applicable to HIT solar cells metallization. In: 2016 IEEE 43rd Photovoltaic Specialists Conference (PVSC); 2016; pp. 2949-2951
- [58] Sinha A, Sharma B. Preparation of copper powder by glycerol process. *Materials Research Bulletin*. 2002;**37**:407-416
- [59] Chow G, Kurihara L, Kemner K, Schoen P, Elam W, Ervin A, Keller S, Zhang Y, Budnick J, Ambrose T. Structural, morphological, and magnetic study of nanocrystalline cobalt-copper powders synthesized by the polyol process. *Journal of Materials Research*. 1995;**10**:1546-1554
- [60] Kobayashi Y, Inose H, Nakagawa T, Gonda K, Takeda M, Ohuchi N, Kasuya A. Control of shell thickness in silica-coating of au nanoparticles and their X-ray imaging properties. *Journal of Colloid and Interface Science*. 2011;**358**:329-333
- [61] Dong Q, Huang C, Duan G, Zhang F, Yang D. Facile synthesis and electrical performance of silica-coated copper powder for copper electronic pastes on low temperature co-fired ceramic. *Materials Letters*. 2017;**186**:263-266
- [62] Schörner S, Clement C, Bell H, Gierth P, Rebenklau L. Industrial inert drying system for high efficiency heterojunction solar cells. In: 31st European Photovoltaic Solar Energy Conference and Exhibition; 2015; Germany, Hamburg. pp. 887-889
- [63] Roncali J. Conjugated poly (thiophenes): Synthesis, functionalization, and applications. *Chemical Reviews*. 1992;**92**:711-738
- [64] Roncali J, Garnier F, Lemaire M, Garreau R. Poly mono-, bi-and trithiophene: Effect of oligomer chain length on the polymer properties. *Synthetic Metals*. 1986;**15**:323-331
- [65] Winter I, Reese C, Hormes J, Heywang G, Jonas F. The thermal ageing of poly (3, 4-ethylenedioxythiophene). An investigation by X-ray absorption and X-ray photoelectron spectroscopy. *Chemical Physics*. 1995;**194**:207-213

- [66] Yabuki A, Arriffin N. Electrical conductivity of copper nanoparticle thin films annealed at low temperature. *Thin Solid Films*. 2010;**518**:7033-7037
- [67] Khanna P, Gaikwad S, Adhyapak P, Singh N, Marimuthu R. Synthesis and characterization of copper nanoparticles. *Materials Letters*. 2007;**61**:4711-4714
- [68] Liu X, Zhou Y. Electrochemical synthesis and room temperature oxidation behavior of cu nanowires. *Journal of Materials Research*. 2005;**20**:2371-2378
- [69] Chen C-H, Yamaguchi T, Sugawara K-i, Koga K. Role of stress in the self-limiting oxidation of copper nanoparticles. *The Journal of Physical Chemistry B*. 2005;**109**:20669-20672
- [70] Foresti E, Fracasso G, Lanzi M, Lesci IG, Paganin L, Zuccheri T, Roveri N. New thiophene monolayer-protected copper nanoparticles: Synthesis and chemical-physical characterization. *Journal of Nanomaterials*. 2008;**2008**:62
- [71] Magdassi S, Grouchko M, Kamyshny A. Copper nanoparticles for printed electronics: Routes towards achieving oxidation stability. *Materials*. 2010;**3**:4626-4638
- [72] Pyo Y, Choi D, Son Y-H, Kang S, Yoon EH, Jung S-B, Kim Y, Lee CS. Fabrication of high quality carbonaceous coating on cu nanoparticle using poly (vinyl pyrrolidone) and its application for oxidation prevention. *Japanese Journal of Applied Physics*. 2016;**55**:055001
- [73] Bokhonov B, Novopashin S. In situ investigation of morphological and phase changes during thermal annealing and oxidation of carbon-encapsulated copper nanoparticles. *Journal of Nanoparticle Research*. 2010;**12**:2771-2777
- [74] Hao C, Xiao F, Cui Z. Preparation and structure of carbon encapsulated copper nanoparticles. *Journal of Nanoparticle Research*. 2008;**10**:47-51
- [75] Jacob DS, Genish I, Klein L, Gedanken A. Carbon-coated core shell structured copper and nickel nanoparticles synthesized in an ionic liquid. *The Journal of Physical Chemistry B*. 2006;**110**:17711-17714
- [76] Li H, Kang W, Xi B, Yan Y, Bi H, Zhu Y, Qian Y. Thermal synthesis of cu@ carbon spherical core-shell structures from carbonaceous matrices containing embedded copper particles. *Carbon*. 2010;**48**:464-469
- [77] Li J, C-y L. Carbon-coated copper nanoparticles: Synthesis, characterization and optical properties. *New Journal of Chemistry*. 2009;**33**:1474-1477
- [78] Gao MR, Xu WH, Luo LB, Zhan YJ, Yu SH. Coaxial metal nano-/microcables with isolating sheath: Synthetic methodology and their application as interconnects. *Advanced Materials*. 2010;**22**:1977-1981
- [79] Wang S, He Y, Liu X, Huang H, Zou J, Song M, Huang B, Liu C. Novel C/cu sheath/core nanostructures synthesized via low-temperature MOCVD. *Nanotechnology*. 2011;**22**:405704

- [80] Wang S, Huang X, He Y, Huang H, Wu Y, Hou L, Liu X, Yang T, Zou J, Huang B. Synthesis, growth mechanism and thermal stability of copper nanoparticles encapsulated by multi-layer graphene. *Carbon*. 2012;**50**:2119-2125
- [81] Lee YI, Lee KJ, Goo YS, Kim NW, Byun Y, Kim JD, Yoo B, Choa YH. Effect of complex agent on characteristics of copper conductive pattern formed by ink-jet printing. *Japanese Journal of Applied Physics*. 2010;**49**:086501
- [82] Eiroma K, Auvinen A, Forsman J, Hult E-L, Jokiniemi J, Koskela P, Sarlin J, Sipiläinen-Malm T, Tapper U. Development of conductive carbon coated copper nanoparticle inkjet fluid. *NIP & Digital Fabrication Conference*; 2011; pp. 458-461
- [83] Dang ZM, Zhang B, Li J, Zha JW, Hu GH. Copper particles/epoxy resin thermosetting conductive adhesive using polyamide resin as curing agent. *Journal of Applied Polymer Science*. 2012;**126**:815-821
- [84] Ohnishi S, Nakasuga A, Nakagawa K. Synthesis of copper particles covered with cobalt-catalyzed carbon nanofibers and their application to air-curable conductive paste. *Japanese Journal of Applied Physics*. 2017;**56**:07KD03
- [85] Gierth P, Rebenklau L, Paproth A, Bell H, Clement C, Vogg F, Sontag D, Mehlich H, Hausmann J, Stein W. Influence of inert curing on polymer paste characteristics on high efficiency heterojunction solar cells. In: *Proceedings of the 28th European Photovoltaic Solar Energy Conference and Exhibition*; Paris. pp. 460-463
- [86] Chapiro A. Radiation chemistry of polymers. *Radiation Research Supplement*. 1964; **4**:179-191
- [87] Nakamura K, Takahashi T, Ohshita Y. Novel silver and copper pastes for n-type bi-facial PERT cell. In: *31st European Photovoltaic Solar Energy Conference and Exhibition*; 2015; Hamburg, Germany. pp. 536-539
- [88] Yoshida S, Dhamrin M, Yoshida M, Uzum A, Itoh U, Tokuhisa H, Sekine S, Saitoh T, Kamisako K. Cost-effective front contact metalization by copper paste for screen-printed crystalline silicon solar cells. In: *Proceedings of the 27th European Photovoltaic Solar Energy Conference and Exhibition*; 2012; Frankfurt, Germany. pp. 1730-1732



# We are IntechOpen, the world's leading publisher of Open Access books Built by scientists, for scientists

6,300

Open access books available

171,000

International authors and editors

190M

Downloads

Our authors are among the

154

Countries delivered to

TOP 1%

most cited scientists

12.2%

Contributors from top 500 universities



WEB OF SCIENCE™

Selection of our books indexed in the Book Citation Index  
in Web of Science™ Core Collection (BKCI)

Interested in publishing with us?  
Contact [book.department@intechopen.com](mailto:book.department@intechopen.com)

Numbers displayed above are based on latest data collected.  
For more information visit [www.intechopen.com](http://www.intechopen.com)



---

# Efficient Low-Cost Materials for Solar Energy Applications: Roles of Nanotechnology

---

Williams S. Ebhota and Tien-Chien Jen

Additional information is available at the end of the chapter

<http://dx.doi.org/10.5772/intechopen.79136>

---

## Abstract

The generation of energy to meet the increasing global demand should not compromise the environment and the future. Therefore, renewable energies have been identified as potential alternatives to fossil fuels that are associated with CO<sub>2</sub> emissions. Subsequently, photovoltaic (PV) solar system is seen as the most versatile and the largest source of electricity for the future globally. Nanotechnology is a facilitating tool that offers a wide range of resources to resolve material challenges in different application areas. This studies X-rays, energy trilemma, potential nanotechnology-based materials for low-cost PV solar cell fabrication, and atomic layer deposition (ALD). In pursuance of improved performance, PV solar-cell technologies have revolutionized from first-generation PV solar cells to third-generation PV solar cells. The efficiency (19%) of second-generation PV cells is higher than the efficiency (15%) of first-generation cells. The second-generation PV cell technologies include a-Si, CdTe and Cu(In,Ga)Se<sub>2</sub>, Cu(In,Ga)Se<sub>2</sub> (CIGS) cells. The third-generation PV cells are organic-inorganic hybrid assemblies, nanostructured semiconductors, and molecular assemblies. This nanocomposite-based technology aims at developing low-cost high efficiency PV solar cells. The nanotechnology manufacturing technique, ALD, is seen as the future technology of PV solar cell production.

**Keywords:** photovoltaic cell low-cost materials, photovoltaic solar technologies, energy trilemma, CO<sub>2</sub> emission, greenhouse gas emission

---

## 1. Introduction

The available energy resources are becoming significantly more interesting due to the transition of the world's energy systems. This transition is orchestrated by the falling

---

technology costs and the improved energy conversion and storage efficiency, coupled with the world stands on greenhouse gas emissions. These trends are expected to continue, with renewables playing a key role. Policymakers and regulatory frameworks of many countries must respond quickly and appropriately to catch up with technology alternatives and unstable energy demands. In a survey, over 50% of energy leaders predicted

Disruptors	Need trend
African economic growth	Demand generation Growing commercial & industrial sector Emerging middle class Access to electricity
Shifting the energy mix	New capital Wind, solar, biomass Gas to power Nuclear Coal Hydro
Changing role of customers	Customer shift Consumer to producer Self-generation Demand managers Every company is an energy company
Renewable technology	Renewable technology Affordability of new technologies Solar PV, storage Off-grid solutions
Smart grids, smarter utilities	Smart utilities Smarter utility management Analytics Smart grids Smart metering
Changing market structures and dynamics	Market restructure Consumer to producer Self-generation Demand managers Every company is an energy company

**Table 1.** Trends of power disruption in SSA [5].

that in 2025 the share of installed distributed generation capacity will increase by 15% or higher [1]. Basden et al. simply put the estimate as 'a business or a home in North America and Europe goes solar every two minutes' [2]. In 2002, United Nations Development Programme estimated the amount of energy that strikes the earth from the sun per year is 1575–49,837 exajoules (EJ). This is by far more than the world's annual energy consumption of about 559.8 EJ [3]. It was posited in Gratzel study in 2001 that covering 0.1% of the earth's surface with PV panels of 10% efficiency will generate the world's total energy need [4]. And yet the developing countries of Africa and other regions are wallowing in energy poverty leading to high unemployment, abject poverty and terrifying standard of living. Till date the energy generated from the sun is less than 0.1% of the current global energy need.

The energy generated from the sun is limited by certain factors which include cost of producing solar cells and the PV cell converting efficiency. To raise the conversion efficiency of solar materials has attracted a lot of interest. Previous attempts to reduce the effects of these factors yielded successes and studies are still on going to break more grounds. The attempts have been multi-criteria improvement approach, which has led to the three categories of PV cell materials today – first, second and third generations of PV materials. However, the world's quest to replace fossil fuels with alternative energy sources has further stretched study on solar materials and system. Several interventions to alter the present power situation in most developing regions, especially in sub-Saharan Africa and Asia (South India), have not yielded the expected results. The impacts of the interventions have been engulfed by challenges arising from global technologies landscape changes, which led to several disruptions in the industry. These disruptors have caused a paradigm shift in the industry in SSA and other developing countries, and have been classified into six by Deloitte as presented in **Table 1** [6]. Therefore, a fresh and systematic power infrastructure investment will be needed to meet the current and future energy demand in developing countries. Solar energy is seen as the best option for alternative energy source because of its abundance, and environmental friendliness. This chapter aims to analyze the global energy trends in terms of achievements, challenges and outlooks. The study X-rays global energy accessibility and the role of PV solar cell system in achieving global supply of energy with modern energy attributes. Further, the significance of nanotechnology in enhancing the efficiency of PV solar materials was discussed.

## 2. Global energy challenges

### 2.1. Access to electricity in developing economies

Developing countries across the regions of the world, especially, sub-Saharan Africa (SSA) and Asia experience a high percentage of inadequate, costly and epileptic power supply

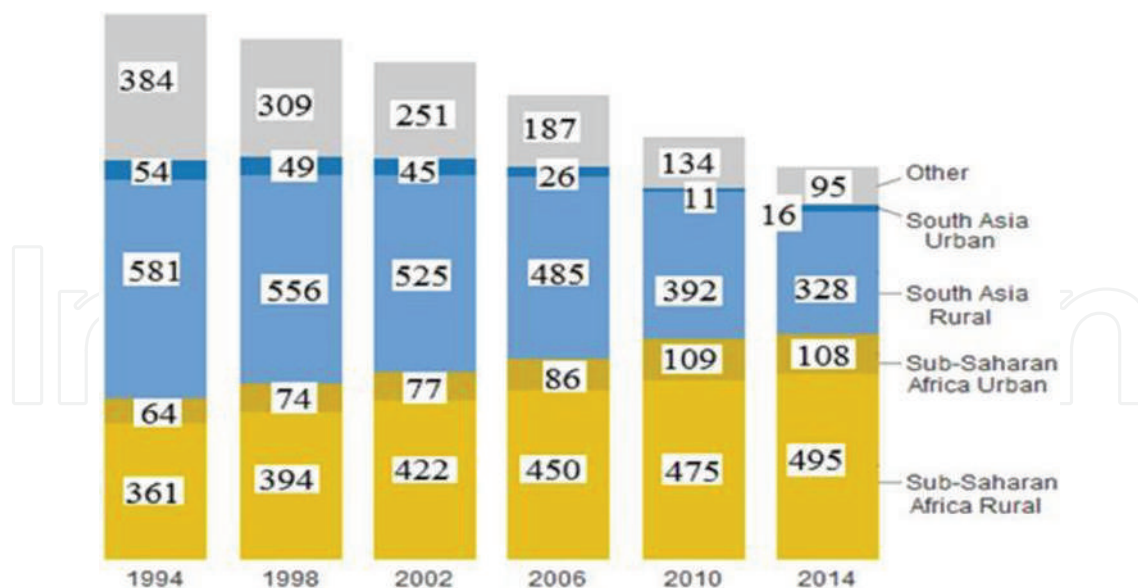


**Figure 1.** People without electricity access in millions in 2014 [9].

[7, 8], as depicted in **Figure 1**. In 2014, the International Energy Agency (IEA) reported that two-thirds of SSA population has no access to electricity and other modern energy services [10]. Large populations have no access to modern energy in many rural and remote areas of developing countries. It has been predicted that the population without access to electricity in rural areas of SSA would increase from 585 million in 2009 to 645 million in 2030 [11]. The concerted efforts and interventions from both domestic and international arenas to change this scenario have not yielded the expected results.

## 2.2. Environment sustainability: fossil fuel global environmental challenges

The world's energy demand from fossil fuels accounts for the upward trend in CO<sub>2</sub> emissions, as shown in **Figure 2**. The fossil fuels for power generation are characterized by climate change, greenhouse gases (GHG) emission, and global warming. In 2012, power and transport sectors generated two-thirds of the global CO<sub>2</sub> emission with each emitting about 42% and 23% respectively [13]. For decades, fossil fuels, such as diesel, petrol, coal, and natural gas have proved to be efficient economic development drivers but with health and environmental consequences. Fossil fuels environmental challenges include climate change, global warming, and CO<sub>2</sub> emissions. These negative fallouts have not deterred man from fossil fuel usage because of energy significance to human existence and industrialization. The world's oil consumption annual growth rate of 1.6%, and gas annual growth rate of 1.5% were reported in 2016 [14].

The amount of GHG emission is vastly different amongst countries but is associated with industrialization. The annual CO<sub>2</sub> emissions from fossil fuels combustion have abruptly risen since the Industrial Revolution from near zero to more than 33 GtCO<sub>2</sub> in 2015. The highly industrialized countries contribute most to CO<sub>2</sub> emission. The International Energy Agency in 2015 estimated the CO<sub>2</sub> emission from industrial waste and non-renewable municipal waste and the combustion of natural gas, oil, coal and other fuels [15]. **Figure 3** shows 20 of the different countries examined.

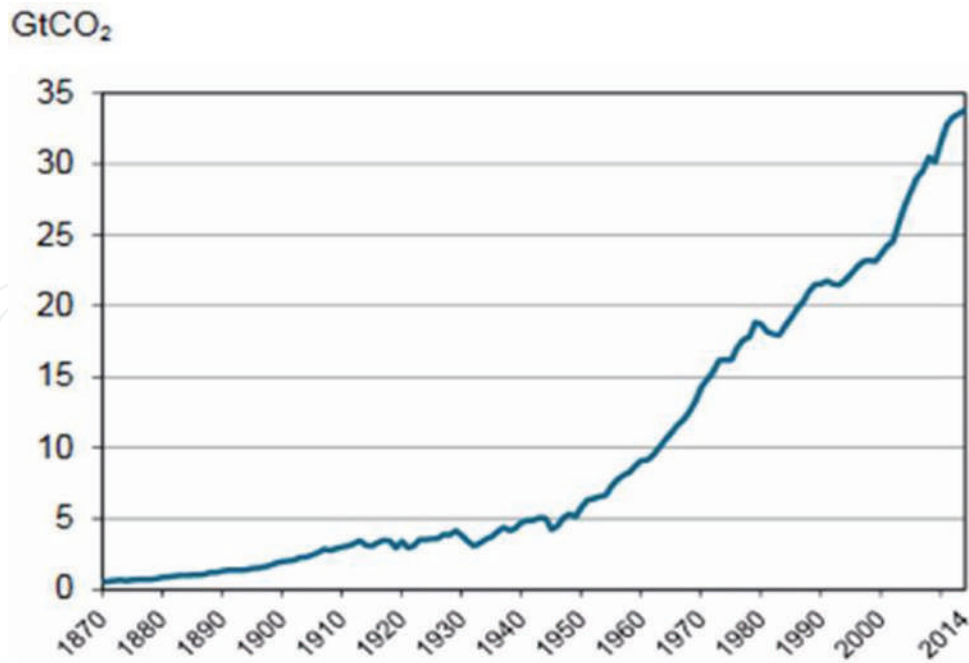


Figure 2. The trend of CO<sub>2</sub> emissions from fossil fuel combustion from 1870 to 2014 [12].

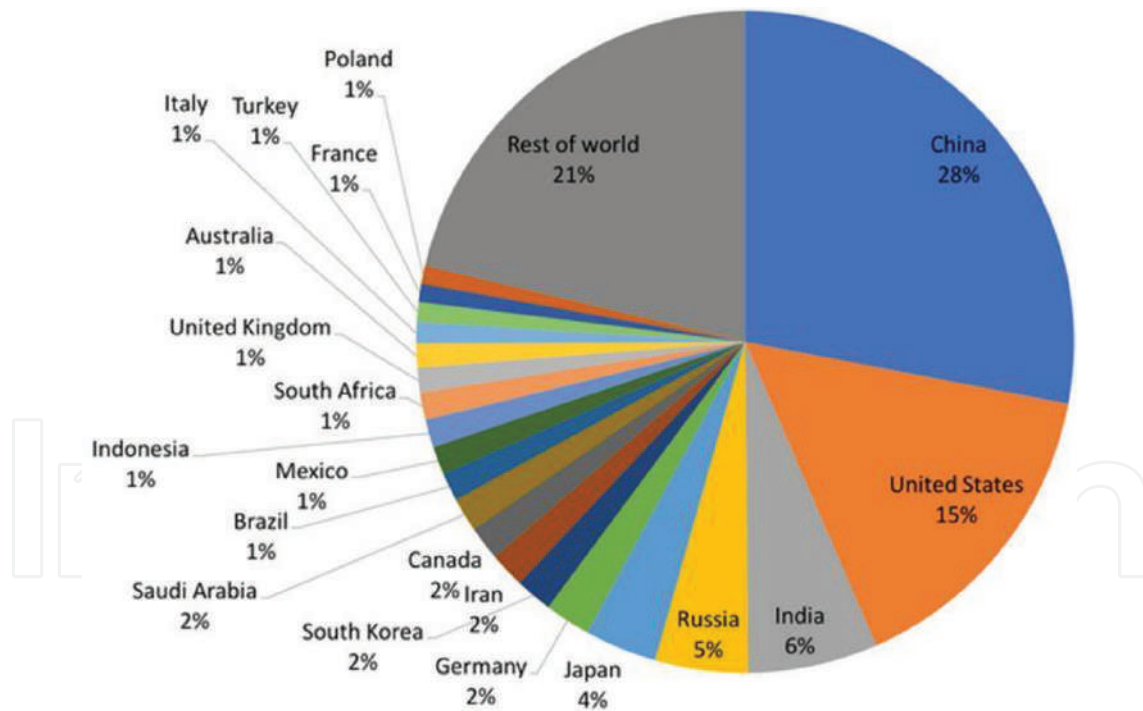
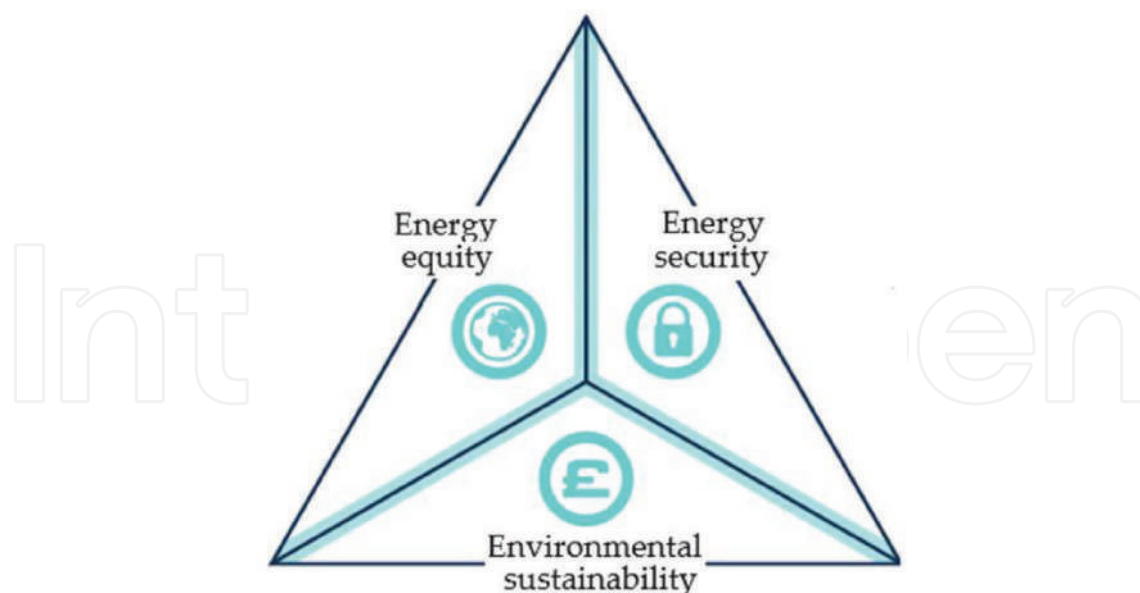


Figure 3. Estimated CO<sub>2</sub> emission of 20 different countries [15].

### 2.3. Energy trilemma

Apart from the need for adequate, and affordable power supply, the global dynamics in the transformation of electricity sector are these three reinforcing trends—digitization, de-carbonization and decentralization. Also, there is an emergence of authorized energy consumers with new choices in how they utilize and manage their energy usage. The governance and



**Figure 4.** The energy trilemma [16].

management of this complex global energy dynamic is challenging and critical to energy security, climate change mitigation and energy poverty. The interconnectivity between energy security, energy equity and environmental sustainability energy poverty, as shown in **Figure 4**, is termed energy trilemma. Energy sustainability was defined by the World Energy Council based on energy security, energy equity, and environmental sustainability [17–19]. Balancing these three dimensions constitutes what is known as energy trilemma and is the foundation for the individual countries' success and competitiveness [16].

The challenge of balancing energy affordability, energy security, and environmental sustainability could promote the understanding of the framework of the disruptions and opportunities of increased decentralization in the energy system. **Table 2** presents opportunities and challenges associated with trilemma.

Components of trilemma	Opportunities	Challenges
Energy security	Energy supply shocks due to improved system resilience can be cushioned by diversification and decentralization of energy sources.	Challenges to system management and the possibility of system failure are promoted by the increased system complexity and technology needs.
Energy equity	Rural electrification and energy democratization can be improved by the range of models of energy supply.	Costs increase may be occurred for system and structure establishment to accommodate the increased system complexity and technology needs.
Environmental sustainability	Alterations in the energy mix have the potential to contribute towards environmental degradation reduction, de-carbonization, and reduce lifecycle impacts known with certain energy sources.	Changes to the energy mix have the potential to increase carbon emissions and create life cycle impacts associated with certain energy sources.

**Table 2.** Trilemma opportunities and challenge.

### 3. Response to global energy and environmental challenges

To appropriately respond to these global challenges, the need to generate more energy without compromising the future becomes a clarion call. This implies the use of fossil fuel should be limited or eliminated. To effectively do this, clean, reliable and renewable energy sources of energy with low or no GHG emissions must be available. To significantly contribute to the realization of global energy trilemma, both developed and developing countries should incorporate the following into their national infrastructure planning:

- Increasing share of renewables
- Electrification of vehicles and process heat by renewable energy sources
- Robust policy framework and consumer sensitization agenda on energy efficiency to reduce GHG emission, costs and risks
- Strengthening the interdependency and complexity of power systems
- Vibrant consumers' awareness program of new energy alternatives
- Greater accessibility and reliable power supply because of growing dependency on electricity
- The rising threat of cyber-attacks should be met with increased energy infrastructure automation
- The introduction of more disruptive technologies, such as energy storage, PV solar, electric vehicles, and power electronics that might substantially change the energy space as the cost of technology drops.

#### 3.1. Alternative energies-clean energies

Renewable energies have been identified as potential alternatives to fossil fuels. This is due to the notable environment benefits the renewable energies offer, such as reduced CO<sub>2</sub> emission and their off grid utilization. Subsequently, the renewable energy technologies are receiving immense attention. The building of renewable technologies infrastructure to increase the portion of electricity generated from renewable energy has commenced in many countries. Policies and framework have been formulated by different countries to guide the use, the growth and the constitutionality of renewable energy. For example, a bill requiring all the electricity retail sellers to serve 33% of their load with renewable energy by 2020 was signed by the governor of California in 2011 [20].

The available alternatives to the fossil fuels are solar, geothermal, tidal, biofuels, hydro, and wind. A huge capacity of the required electricity can be derived from nuclear energy. However, many countries are skeptical about the use of nuclear energy because of the perceived side effects. They consider the use of nuclear energy for electricity as a risky venture. In Singapore for instance, studies by independent analysts and government agencies have described the existing nuclear plants as too risky for Singapore's small size and dense population [21]. Amongst these natural resources sun (solar), small hydropower, and wind are the

most established and are considered better alternatives for environment and cheaper electricity sources in the long term. The exploitability of the solar resource in urbanization is more versatile than other renewable energy sources.

### 3.1.1. Solar energy: photovoltaic solar cell

Criticisms have trailed renewable energy technology due to their low energy densities, intermittency and region-based resources, making them less suitable for urban applications. Solar is the most common renewable energy whose potential is highly region-dependent. However, the annual direct solar irradiation in some regions exceeds  $300 \text{ W/m}^2$ . Interestingly, several of the regions that are likely to experience the maximum increase in urbanization are in solar-rich regions. Subsequently, a lot of studies and technical advances have been focused on solar efficiency, structure and cost. This resulted in a drastic drop of solar energy installed price by about 50% since 2010 [22]. Despite this achievement, the efficiency of multi-crystalline silicon photovoltaic cell, which is the widely installed panels, is hovering around 10–17% [23]. However, recent studies have shown PV laboratory efficiency over 40%, using concentrated multijunction cells [24]. This means that the photovoltaics power density could surpass  $120 \text{ W/m}^2$  under optimal conditions. For instance, Singapore has an annual average of solar irradiance of  $1580 \text{ kWh/m}^2/\text{year}$  and about 50% more solar radiation than temperate countries. This makes solar photovoltaic (PV) generation as the greatest potential for wider utilization in Singapore. In 2014, Singapore planned to raise solar power from 19 MWp installed capacity to 350 MWp by 2020 and this is 5% of the projected peak electricity demand [25].

The world solar heat collectors' thermal power density average is  $67 \text{ Wt/m}^2$  [23, 26] and the use of domestic solar hot-water heaters is on the increase because it is low-cost and compact. Up to 84% of urban households installed solar hot-water heaters on their rooftops [27] and five Australian cities saving approximately 17% energy, using a Trombe wall. Trombe is a technique of collecting and storing of solar thermal energy in the summer for heating in the winter. About 91% of the total energy required in a large residential building in Richmond, VA, is provided from this technology [28].

## 3.2. Sustainable integrated policies and technologies for urbanization

Sustainable development challenges come with a rise in global urbanization in the dense cities especially in the lower-middle-income countries where the growth of urbanization is rapid. Urban sustainable solutions in the form of integrated policies and technologies are needed globally to lower GHG emissions, reduce the cost of clean energy and guarantee safe energy. The common clean energy challenges in urban are energy intermittency and reliability, cost of installation and low power density. Renewable energies such as wind, hydro and solar have common intermittency and reliability challenges. It is not always windy, sunny and the water level in the source is not always the same. This limits the level of providing a constant power supply to users. There are several approaches that are ongoing in tackling these challenges and these include: the combination of renewable energy sources in a hybrid system; and development of low-cost and efficient renewable energy generation and storage materials.

### 3.3. Hybrid renewable energy systems

The goal of the combined systems is to cushion the inconsistency supply by a power bolster, either a diesel generator or pumped storage hydroelectric. The bolster runs at low output during low peak hours' demand and increases to full output at peak hours' demands. The combination of renewable energy sources, such as solar, hydro, wind, diesel generator and energy storage units, have been studied extensively in recent years. This combination is often called hybrid renewable energy systems (HRES). Hybrid renewable energy system is a response to challenges of scarce supply of a single renewable resource and intermittent generation challenges. The study on HRES involves modeling, managing and optimizing the different energy systems from design to operation, as shown in **Figure 5** [30–34]. It is vital to consider the system design and operation from a range of time scales because HRES has various stages of life cycle. Irrespective of life cycle (whole life or daily), real-time optimization offers a significant opportunity to handle HRES systematically [29].

The attainment of clean energy based urbanization, large depends on the advances in renewable energy generation technologies, in terms of low cost and efficiency. For a faster, more secure transition from fossil fuels, high efficient and low-cost renewable energy generation and storage materials need to be developed.

### 3.4. Photovoltaic solar systems

The photovoltaic solar system is composed of different supporting components in addition to PV solar modules. This supporting equipment, often referred to as balance of system (BOS), serves to balance the system and to sustain the operation. The BOS components include controllers, energy storage devices, wiring, grid connections, trackers, mounting hardware, and inverters. However, these components vary from one system to another depending on the scale and application. The different types of PV configurations that work for both Grid-connected and Stand-alone applications are shown in **Figure 6**.

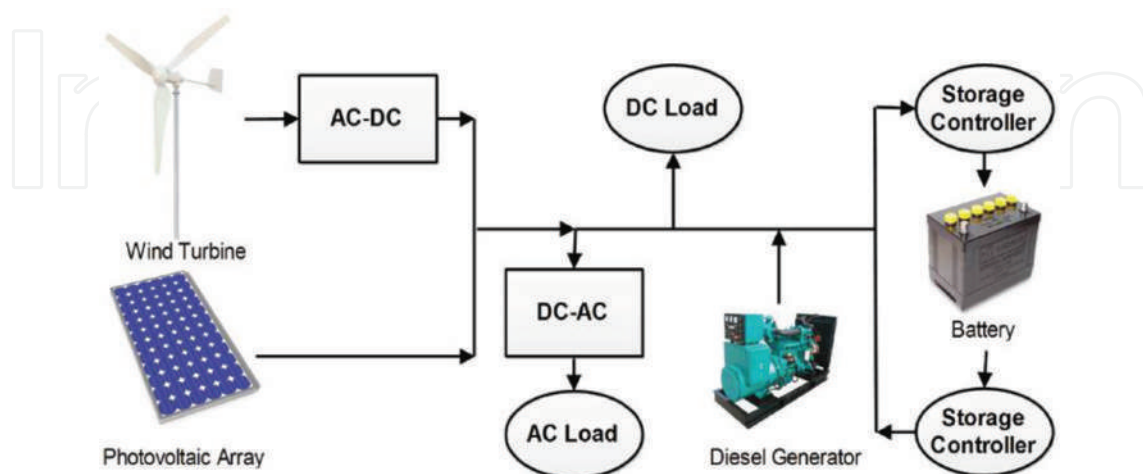


**Figure 5.** Hybrid renewable energy system (HRES) schematic [29].

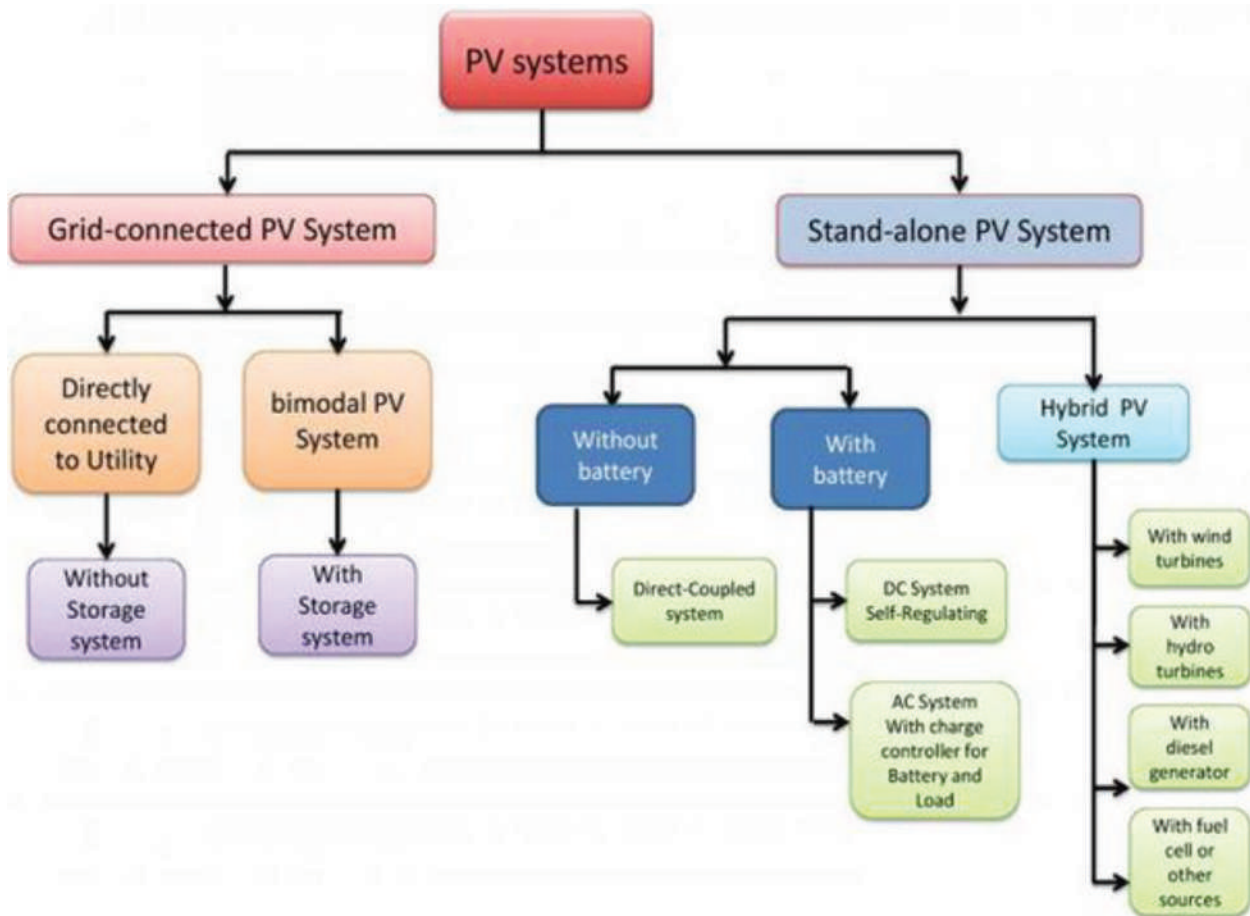


**Figure 6.** The different types of PV configurations [35].

During repairs, the BOS components can be removed or added to the plant without significant disruption to the infrastructure due to the modular nature of PV solar system. The balance of system components and their functions are presented in **Table 3**. The quality of the BOS is crucial for providing efficient and lasting operation, as the industry aim is to offer PV systems with minimum operational lifetime of 25 years [36, 37]. **Figure 7** shows photovoltaic solar system.

There are three basic processes of photovoltaic effect and they are:

- i. Production of charge carriers because of the absorption of photons in the materials that make a junction.
- ii. The resulting parting of the photo-generated charge carriers in the junction.
- iii. Collection of the photo-generated charge carriers at the terminals of the junction.

The solar cells working principle is based on the production of a potential difference at the junction of two different materials in response to electromagnetic radiation photovoltaic, as shown in **Figure 8**. This occurrence is generally termed photovoltaic effect and is similar to photoelectric effect, which is the emission of electrons from materials that absorb light at a frequency that exceeds the material-dependent threshold frequency. Albert Einstein in 1905 explained this effect has energy and assumed that the light has well-defined energy quanta, called photon, given as Eq. (1):

$$E = hv \tag{1}$$

The absorption of photon by a semiconductor with a bandgap,  $E_g$  is shown in **Figure 8**. The photon with energy  $E_{ph} = h\nu$  excites an electron from  $E_i$  to  $E_f$ . At  $E_i$  a hole is created. If  $E_{ph} > E_g$  a part of the energy is thermalized.

where  $h$  is Planck's constant and  $\nu$  is the light frequency.

Component	Functions
Battery	The electrical power harvested by PV solar panels can be stored in batteries. Solar systems are often built with a battery backup to be used at night or dull days. The batteries are usually deep cycle batteries because of their robustness and discharging endurance.
Battery charge controllers	The battery charge controller is similar to automotive battery charger in function. It ensures that a consistent amount of power is sent to the batteries to avoid over charged, and to prevent the backup battery from discharging back through the system at night.
Inverter—solar power converter	It converts the solar panels generated DC power into AC power using electronic switching techniques since home runs on AC power.
Trackers	A device for concentrating a solar reflector, orienting a solar panel or lens towards the sun for optimization of solar energy conversion into electricity.
Mounting hardware	The solar panels are placed on mounting hardware.
Main panel	This is where all electric loads in the building are connected, and protected with circuit breakers.
System power meter	Is enhances the system to gain maximum efficiency from solar installation and estimates the amount of money being saved by the solar system.
Power conditioning unit	It offers protection against electric faults, such as short line-to-ground faults or circuits.
DC and AC disconnect	Solar systems are usually provided with manual disconnection devices for safety reasons. They are used to cut off the power during maintenance and emergency.

**Table 3.** Functions of photovoltaic solar system components.

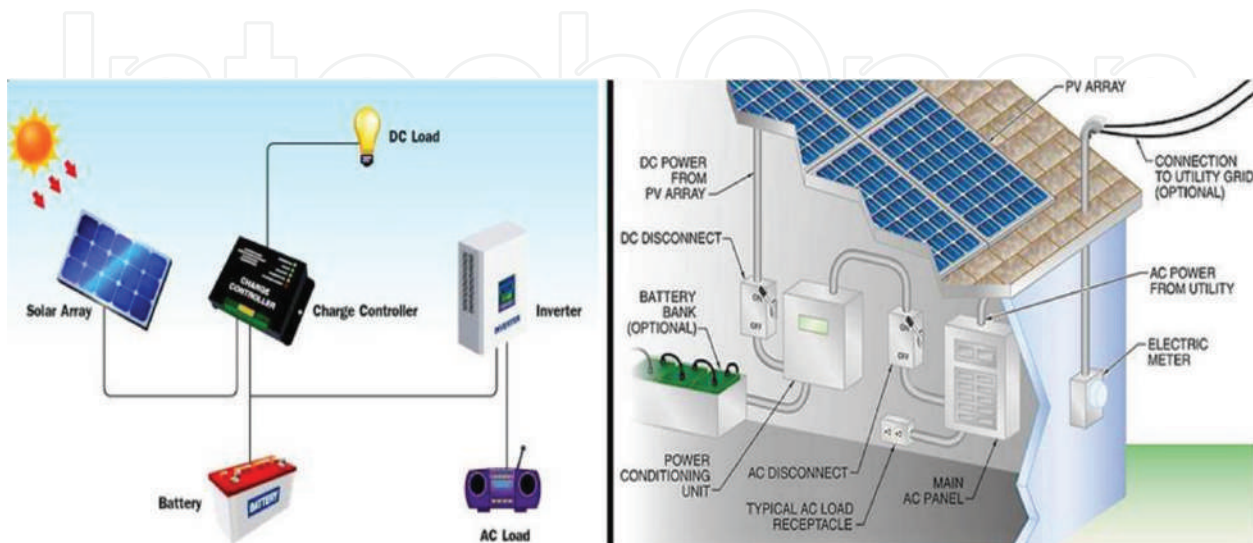


**Figure 7.** The photovoltaic solar system [38, 39].

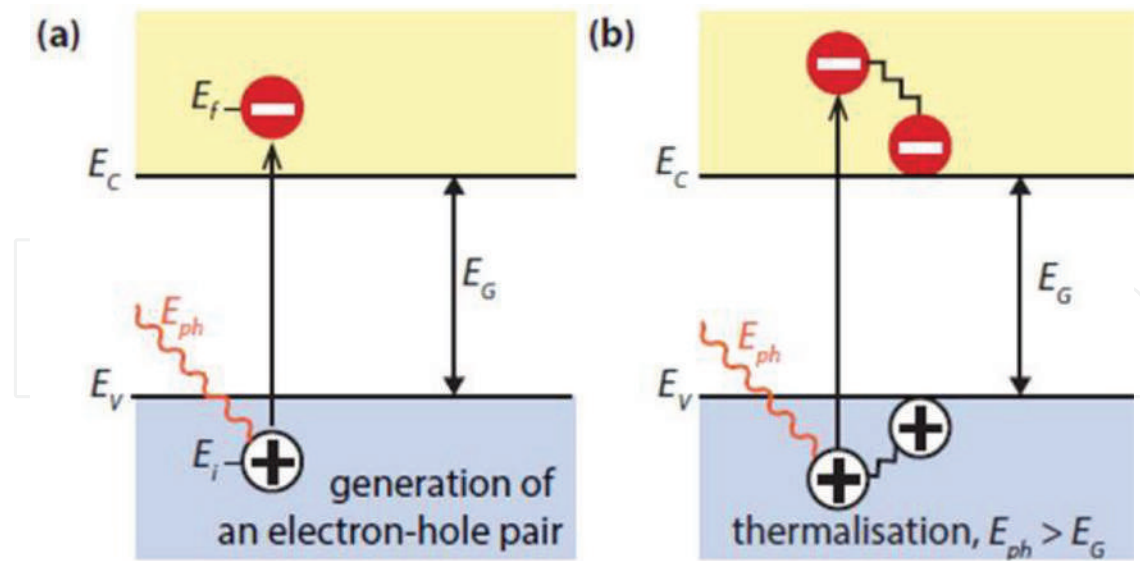


**Figure 8.** (a) Depicts semiconductor absorption of a photon with bandgap  $E_G$ . (b) If  $E_{ph} > E_g$  a part of the energy is thermalized.

## 4. The development of low-cost and efficient renewable energy generation and storage materials

There has been an intense study on the development of low-cost and efficient renewable energy generation and storage materials, but the scope of work only covers PV cell materials. The application of photovoltaic (PV) technology to harness the huge amounts of energy that the sun releases to the earth is one of the most promising alternatives. Thin-film or crystalline silicon are the most widely used materials for industrial production of PV cells [40]. However, the rigidity form of Si PV modules limits their economic incorporation into commercial and residential buildings, while thin film PV cells are more appropriate in terms of cost, ease of fabrication and installation [41]. The thin film PV is receiving more attention and is being considered for large scale power generation and for building integrated photovoltaic (BIPV) applications [42].

### 4.1. Encapsulation of thin film PV cells

Photovoltaic modules are desirable to provide cheap power for more than 20 years at <10% power degradation outputs at an affordable production cost [43]; and survive 1000 hours at ambient conditions of 85°C and 85% relative humidity in accordance with IEC61646 international standard [44]. Providing thin layer barriers to protect thin film CIGS and DSSC to satisfy these requirements has been challenging. This is because both cells degrade under the ambient conditions if they are not properly protected from moisture ingress.

The requirement for efficient methods to module encapsulation, is a serious challenge facing thin film PV modules producers. The quest to develop appropriate approach for thin film cells encapsulation started around 2002 and is still ongoing. Hence, new low-cost methods of module encapsulation are required to meet this desire. Present developments in the PV cells industry have affected the initial barrier coatings. DSSC and CIGS on flexible substrates are

now being considered for flat plate modules with glass-to-glass and BIPV as well as for flat plate module applications, respectively.

#### 4.2. Photovoltaic module materials

Copper indium gallium selenide (CIGS) – one of the most recent developed materials in the renewable energy space, are copper indium gallium selenide,  $\text{CuIn}_{1-x}\text{Ga}_x\text{Se}_2$  (CIGS) materials, used for flexible thin-film photovoltaic (PV) modules. Their efficiency levels are beyond that of Si-based rigid PV modules and the films offer substantial advantages in the mass and building integrated photovoltaic (BIPV) applications. However, they are greatly susceptible to environmental degradation in the long term due to water vapor transmission to the active (absorber) layer via the protective encapsulation layer. To prevent the permeability of water vapor to the absorber, a barrier layer of a few nanometres thickness is provided to encapsulate the PV. Roll-to-roll (R2R) atomic layer deposition (ALD) methods are used to deposit amorphous aluminum oxide ( $\text{Al}_2\text{O}_3$ ) material on a planarized polyethylene naphthalate (PEN) substrate. However, water vapor still permeates the barrier because of micro and nano-scale defects present, generated by the deposition process. This occurrence reduces the cell efficiency unit longevity, and ultimately, causes failure [45]. Roll-to-roll technology is used to manufacture flexible devices by repeatedly depositing and patterning of thin layer materials on polymer films substrates [46]. The thickness of the flexible thin layer prior to final encapsulation is about  $3\ \mu\text{m}$  [47].

In the solar community, apart from CIGS, dye-sensitized solar cells (DSSCs) have attracted interest and are being given considerable attention due to these attributes: ease of production, comparatively low fabrication cost; and reasonable solar-to-electrical efficiency. Subsequently, they have been regarded as potential materials to replace traditional Si-based solar cells in specialized applications [48]. However, there is a limitation on the absorption coefficient due to standard DSSC employment of a Ru-based dye, which possesses moderate molar absorption [49, 50]. The DSSC system therefore, requires a high surface area substrate for the dye, nanoparticulate  $\text{TiO}_2$ , and to attain good light harvesting efficiency (LHE). Further, a slow redox shuttle usually I-/I3 is needed since electron transport is reasonably slow in nanoparticulate  $\text{TiO}_2$  [51].

### 5. Application of nano based technology in the manufacturing of energy materials

Chapin et al. at Bell laboratories developed the first generation of PV solar cells, silicon (Si) p/n in 1954 [52]. The first generation PV solar cells have high cost as a major drawback due to the quality of materials used - low defect single Si crystal, reinforced low-iron glass cover sheet, and encapsulants. The second generation solar cells were aimed at lowering cost than the first generation. Examples of the second generation cells technologies are a-Si, CdTe and  $\text{Cu}(\text{In,Ga})\text{Se}_2$ ,  $\text{Cu}(\text{In,Ga})\text{Se}_2$  (CIGS) cells. Although, this generation cells have efficiency of 19%, which is higher than the first generation PV cells efficiency, the price is considered high. They are usually use in space applications where cost is not a major drawback [53]. In pursuit of overcome the cost and efficiency challenges associated with PV solar cells, the

concept of nanocomposite, which enhances device for better performance was utilized. This was exploited in the production of PV solar cells to surmount limits of single materials in solar spectrum response; reaction of holes or electrons with chemicals; transport of holes or electrons; and reduce of costs. This gave birth to the third generation devices that are based on nanocomposites, such as organic–inorganic hybrid assemblies, nanostructured semiconductors, and molecular assemblies. The third generation PV solar cells are aiming to deliver low-cost high efficiency materials nanocomposite.

### 5.1. Application of atomic layer deposition

Atomic layer deposition (ALD) is a vapor-phase based deposition technique used for depositing high quality, conformal and uniform thin films at comparatively low temperatures. This technique is used to control interface properties through the deposition of high-quality thin films with specific growth control, excellent uniformity over large areas and very good step coverage on non-planar surfaces [54, 55]. These striking attributes of ALD have been employed in several applications including in the fabrication of solar cells for PV modules. In this regard, ALD has benefited the surface passivation layers, buffer layers and barrier layers of crystalline silicon (c-Si), CIGS and dye-sensitized solar cells (DSSCs). Encapsulation of flexible CIGS and organic photovoltaic (OPV) cells with film layer barriers has been performed successfully with ALD. Presently, ALD has been described as the future standard of solar cell equipment manufacturing.

The application of ALD for PV cell started in the 1990s and Bedair and co-workers group reported the first application in 1994. This was followed by the reports on the use ALD to deposit boron-doped ZnO films as transparent conductive oxide (TCO) and ZnSe buffer layers for CIGS solar cells [56]. In 1998, copper indium diselenide (CIS) cells was acclaimed the most common thin film material for PV [57], while the application of a more productive, similar combination material, CIGS, was reported in 2009 [58]. Thin film PV modules are preferred to the conventional crystalline rigid Si cells mainly because of the following merits:

- i. Thin film PV cells require less materials [59].
- ii. Several vacuum and non-vacuum techniques are used to deposit in thin films PV cells on inexpensive substrates [60].
- iii. Thin film deposition on flexible and/or curved substrates, such as polymeric sheets is achievable, forming rollable or foldable solar generators [61]. This has further increased PV cells application areas to include high altitude platforms, cars, aircraft, and various electric appliances. Flexible PV thin-film offers specific design alternatives for BIPVs [62] and the interest in flexible thin film PV cells and technologies is progressively increasing.

In a study [63], ALD was carefully used to develop CuSbS<sub>2</sub> thin films at a low-temperature route. After 15 minutes, postprocess, annealing, was performed at 225°C. It was observed that CuSbS<sub>2</sub> films ALD-grown, crystalline with micron-sized grains, showed a band gap of 1.6 eV, absorption coefficient of  $>10^4 \text{ cm}^{-1}$ , and hole concentration of  $10^{15} \text{ cm}^{-3}$ . Further, the study demonstrated the first open-circuit voltage on par with CuSbS<sub>2</sub>/CdS heterojunction PV devices and the potential of ALD grown CuSbS<sub>2</sub> thin films in environmentally friendly

PVs. It concluded that  $\text{CuSbS}_2$  and  $\text{Cu}_{12}\text{Sb}_4\text{S}_{13}$ , members of the Cu–Sb–S family that may be reproducibly synthesized by ALD were added to the short list of metal sulfide thin films.

Recently, attention has been given to new mixed metal oxide materials realized from templating strategy in combination with ALD for DSSC photoelectrodes. Hamann et al. [64] showed the feasibility of the use of  $\text{TiO}_2$  structures as dye-sensitized electrodes by typifying their forms and photovoltaic performance. In the study, a new pseudo-one-dimensional structure for DSSC photoanodes was made from mesoporous aerogel, a low-density, high surface area, and thin films by templating. Atomic layer deposition was used to control the variable thickness of  $\text{TiO}_2$  deposition on aerogel templates conformally. The study revealed that the cell efficiency was proportional to  $\text{TiO}_2$  thickness deposited because of increasing charge diffusion lengths; the electrodes integrated into DSSCs showed good light harvesting and exceptional power efficiencies compared with the nanoparticle  $\text{TiO}_2$  based DSSCs; and ALD-coated aerogel-templated photoanodes have been described as a promising candidate to move beyond nanoparticle electrodes in DSSCs due to design flexibility, materials generality, and ease of manufacturing.

## 6. Conclusion

The World Energy Council categorized energy sustainability into three components - energy security, energy equity, and environmental sustainability. Fossil fuels are the greatest economic drivers amongst the available fuels, but they have huge environmental threats and consequences, such as  $\text{CO}_2$  emissions. The increasing global energy demand coupled with the complex nature of the global energy dynamic make management challenging. To effectively respond to the global energy challenges, the generation of energy to satisfy the increasing demand should be done without compromising the environment. Solar energy is a potential alternative to fossil fuel is known for  $\text{CO}_2$  emission. As such, photovoltaic solar system is seen as the best option to fossil fuels. The exploitability of solar resource amongst renewable energy sources and the production of low-cost flexible PV cells will facilitate energy trilemma success.

## Acknowledgements

The authors would like to thank the financial support from National Research Foundation (NRF) of South Africa and Global Excellence Scholarship from the University of Johannesburg.

## Author details

Williams S. Ebhota\* and Tien-Chien Jen

\*Address all correspondence to: [willymoon2001@yahoo.com](mailto:willymoon2001@yahoo.com)

Mechanical Engineering Department, University of Johannesburg, Johannesburg,  
South Africa

## References

- [1] Austin F. Distributed Disruptions in the Energy Sector. 2017 (Apr 14, 2018). Available: <https://www.brinknews.com/distributed-disruptions-in-the-energy-sector/>
- [2] Basden J, Witkowski A, Wright T. The new make vs buy Calculus how utilities can remain relevant to customers who produce their own power. *The Oliver Wyman Energy Journal*. 2016;**2**:19-21
- [3] Wikipedia Contributors. Solar Energy. In: *Wikipedia, The Free Encyclopedia*. 2018. Available from: [https://en.wikipedia.org/w/index.php?title=Solar\\_energy&oldid=841654454](https://en.wikipedia.org/w/index.php?title=Solar_energy&oldid=841654454) [Accessed: May 26, 2018]
- [4] Grätzel M. Photoelectrochemical cells. *Nature*. 2001;**414**:338 (11/15/online)
- [5] Ebhota WS, Tabakov PY. Hydropower potentials and effects of poor manufacturing infrastructure on small hydropower development in sub-Saharan Africa. *International Journal of Energy Economics and Policy*. 2017;**7**:60-67
- [6] Deloitte. Sub-Saharan Africa Power Trends: Power Disruption in Africa. (2015, 14/06/2018). Available: <https://www.deloitte.com/za/en/pages/energy-and-resources/articles/sub-saharan-africa-power-trends.html>
- [7] Mohammed YS, Mustafa MW, Bashir N. Hybrid renewable energy systems for off-grid electric power: Review of substantial issues. *Renewable and Sustainable Energy Reviews*. 2014;**35**:527-539 (Jan 7, 2014)
- [8] Trotter PA. Rural electrification, electrification inequality and democratic institutions in sub-Saharan Africa. *Energy for Sustainable Development*. 2016;**34**:111-129 (Jan 10, 2016)
- [9] Khokhar T. Chart: Globally, the Number of People Without Access to Electricity is Falling. 2017. Available from: <https://blogs.worldbank.org/opendata/chart-globally-number-people-without-access-electricity-falling> [Accessed: Mar 24, 2018]
- [10] IEA. 2014 FACTSHEET Energy in Sub-Saharan Africa Today. Paris, France: International Energy Agency; 2014 (World Energy Outlook)
- [11] IEA (International Energy Agency). *World Energy Outlook 2011*. Paris: OECD/IEA; 2011. Available from: [https://www.iea.org/publications/freepublications/publication/WEO2011\\_WEB.pdf](https://www.iea.org/publications/freepublications/publication/WEO2011_WEB.pdf) [Accessed: Mar 16, 2011]
- [12] IEA. *CO<sub>2</sub> Emissions From Fuel Combustion Highlights*. 2017 ed. France: International Energy Agency (IEA); 2017
- [13] IEA. *CO<sub>2</sub> Emissions From Fuel Combustion Statistics Highlights*. IEA Statistics. 2014 ed. Paris, France: International Energy Agency; 2014
- [14] BP. *Statistical Review of World Energy*. 2017. Available from: <https://www.bp.com/content/dam/bp/en/corporate/pdf/energy-economics/statistical-review-2017/bp-statistical-review-of-world-energy-2017-full-report.pdf>

- [15] IEA. Key Trends in CO<sub>2</sub> Emissions from Fuel Combustion. 2015 ed. France: International Energy Agency (IEA); 2015
- [16] Nottingham L, Neher D, Pasquale G, Buser A, Beaven J, Winkler S, et al. World Energy Trilemma: Changing Dynamics – Using Distributed Energy Resources to Meet the Trilemma Challenge. United Kingdom: World Energy Council; 2017
- [17] Wyman O. World Energy Trilemma: Priority Actions on Climate Change and How to Balance the Trilemma. London, UK: World Energy Council; 2015
- [18] Nentura. Our Energy Trilemma. Apr 2, 2018. Available from: <http://www.rdawep.org.au/wp-content/uploads/2017/03/The-Energy-Trilemma.pdf>
- [19] Tomei J, Gent D. Equity and the Energy Trilemma: Delivering Sustainable Energy Access in Low-Income Communities. London: International Institute for Environment and Development; 2015
- [20] EC. California Renewable Energy Overview and Programs. 2011. Available from: <http://www.energy.ca.gov/renewables/> [Accessed: Dec 3, 2017]
- [21] Zengkun F, Chua G. From The Straits Times Archives: Resolving Singapore's Green Energy Trilemma. 2015. Available from: <http://www.straitstimes.com/singapore/environment/from-the-straits-times-archives-resolving-singapores-green-energy-tri-lemma> [Accessed: Nov 29, 2017]
- [22] U. S. Quadrennial Technology Review: Solar Power Technologies. U.S: U.S. Department of Energy; 2015
- [23] Kammen DM, Sunter DA. City-Integrated Renewable Energy for Urban Sustainability. Nov 30, 2017. Available from: <https://gspp.berkeley.edu/research/featured/city-integrated-renewable-energy-for-urban-sustainability>
- [24] NREL. Transforming Energy through Science. USA: National Renewable Energy Laboratory, Office of Energy Efficiency and Renewable Energy; 2016
- [25] EMA. Solar Photovoltaic Systems. 2017. Available from: [https://www.ema.gov.sg/Solar\\_Photosvtaic\\_Systems.aspx](https://www.ema.gov.sg/Solar_Photosvtaic_Systems.aspx)
- [26] Smil V. Power Density: A Key to Understanding Energy Sources and Uses. USA: MIT Press; 2015
- [27] Wei H, Liu J, Yang B. Cost-benefit comparison between domestic solar water heater (DSHW) and building integrated photovoltaic (Bipv) systems for households in urban China. Applied Energy. Jan 8, 2014;**126**:47-55
- [28] Terziotti LT, Sweet ML, McLeskey JT Jr. Modeling seasonal solar thermal energy storage in a large urban residential building using TRNSYS 16. Energy and Buildings. Feb 2012;**45**:28-31
- [29] Wang X, Palazogluy A, El-Farra NH. Operation of residential hybrid renewable energy systems: integrating forecasting, optimization and demand response. Presented at the American Control Conference (ACC), Portland, Oregon, USA. 2014

- [30] Deshmukh M, Deshmukh S. Modeling of hybrid renewable energy systems. *Renewable and Sustainable Energy Reviews*. 2008;**12**:235-249
- [31] Jung J, Villaran M. Optimal planning and design of hybrid renewable energy systems for microgrids. *Renewable and Sustainable Energy Reviews*. Jan 8, 2017;**75**:180-191
- [32] Sawle Y, Gupta SC, Bohre AK. Socio-techno-economic design of hybrid renewable energy system using optimization techniques. *Renewable Energy*. Nov 21, 2017
- [33] Sawle Y, Gupta SC, Bohre AK. Review of hybrid renewable energy systems with comparative analysis of off-grid hybrid system. *Renewable and Sustainable Energy Reviews*. Jan 1, 2018;**81**:2217-2235
- [34] Wang X, Palazoglu A, El-Farra NH. Operational optimization and demand response of hybrid renewable energy systems. *Applied Energy*. Jan 4, 2015;**143**:324-335
- [35] Chaaban MA. PV System Types and Components. Apr 15, 2018. Available: <https://www.e-education.psu.edu/ae868/node/872>
- [36] Baurzhan S, Jenkins G. On-grid solar PV versus diesel electricity generation in sub-Saharan Africa: Economics and GHG emissions. *Sustainability*. 2017;**9**:372
- [37] Ani VA. Design of a stand-alone photovoltaic model for home lightings and clean environment. *Frontiers in Energy Research*. Jan 11, 2016;**3**: M. A. Chaaban. (15/04/2018). PV System Types and Components. Available: <https://www.e-education.psu.edu/ae868/node/872>
- [38] The Grid Solar. PV Systems: Overview of the Main Components. Apr 10, 2018. Available from: [https://thegrid.rexel.com/en-us/energy\\_efficiency/w/solar\\_renewable\\_and\\_energy\\_efficiency/82/solar-pv-systems-overview-of-the-main-components](https://thegrid.rexel.com/en-us/energy_efficiency/w/solar_renewable_and_energy_efficiency/82/solar-pv-systems-overview-of-the-main-components)
- [39] Leonics. Basics of Solar Cell. Apr 10, 2018. Available from: [http://www.leonics.com/support/article2\\_13j/articles2\\_13j\\_en.php](http://www.leonics.com/support/article2_13j/articles2_13j_en.php)
- [40] Carcia PF, McLean RS, Hegedus S. Encapsulation of Cu(InGa)Se<sub>2</sub> solar cell with Al<sub>2</sub>O<sub>3</sub> thin-film moisture barrier grown by atomic layer deposition. *Solar Energy Materials and Solar Cells*. Jan 12, 2010;**94**:2375-2378
- [41] Ahmad E. Growth and Characterisation of Cu(In, Ga)Se<sub>2</sub> Thin Films for Solar Cell Applications. UK: University of Salford; 1995
- [42] James T, Goodrich A, Woodhouse M, Margolis R, Ong S. Building-integrated photovoltaics (BIPV) in the residential sector: An analysis of installed rooftop system prices. *Contract*. 2011;**303**:275-3000
- [43] Olsen LC. Barrier Coatings for Thin Film Solar Cells Final Subcontract Report. National Renewable Energy Laboratory, Richland, Washington; 2008
- [44] CSZ. Photovoltaic Solar Testing Specifications. Nov 16, 2017. Available from: <http://www.cszindustrial.com/Products/Custom-Designed-Chambers/Solar-Panel-Testing-Chamber/Solar-Testing-Specifications.aspx>

- [45] Grover R, Srivastava R, Rana O, Mehta D, Kamalasanan M. New organic thin-film encapsulation for organic light emitting diodes. *Journal of Encapsulation and Adsorption Sciences*. 2011;**1**:23-28
- [46] Galagan Y, Andriessen R. Organic photovoltaics: Technologies and manufacturing. In: Fthenakis V, editor. *Third Generation Photovoltaics*. Rijeka: InTech; 2012 (Ch. 3)
- [47] Elrawemi M. Metrology and characterisation of defects in thin film barrier layers employed in flexible photovoltaic modules. PhD. Mechanical Engineering, University of Huddersfield: UK, 2015
- [48] Prasittichai C, Hupp JT. Surface modification of SnO<sub>2</sub> photoelectrodes in dye-sensitized solar cells: Significant improvements in photovoltage via Al<sub>2</sub>O<sub>3</sub> atomic layer deposition. *The Journal of Physical Chemistry Letters*. May 20, 2010;**1**:1611-1615
- [49] Martinson ABF, Hamann TW, Pellin MJ, Hupp JT. New architectures for dye-sensitized solar cells. *Chemistry – A European Journal*. 2008;**14**:4458-4467
- [50] Hamann TW, Jensen RA, Martinson ABF, Van Ryswyk H, Hupp JT. Advancing beyond current generation dye-sensitized solar cells. *Energy & Environmental Science*. 2008;**1**:66-78
- [51] Martinson AB, Goes MS, Fabregat-Santiago F, Bisquert J, Pellin MJ, Hupp JT. Electron transport in dye-sensitized solar cells based on ZnO nanotubes: Evidence for highly efficient charge collection and exceptionally rapid dynamics. *The Journal of Physical Chemistry A*. Apr 23, 2009;**113**:4015-4021
- [52] Chapin DM, Fuller CS, Pearson GL. A new silicon P-N junction photocell for converting solar radiation into electrical power. *Journal of Applied Physics*. 1954;**25**:676-677
- [53] Cheng Z. *Solar Nanocomposite Materials, Advances in Nanocomposite Technology*. London, United Kingdom: IntechOpen; 2011
- [54] Puurunen RL. Surface chemistry of atomic layer deposition: A case study for the trimethylaluminum/water process. *Journal of Applied Physics*. Jun 15, 2005;**97**:121301
- [55] George SM. Atomic layer deposition: An overview. *Chemical Reviews*. Jan 13, 2010; **110**:111-131
- [56] Yasutoshi O, Katsumi K, Mitsuru I, Akira Y, Makoto K. Polycrystalline Cu(InGa)Se<sub>2</sub> thin-film solar cells with ZnSe buffer layers. *Japanese Journal of Applied Physics*. 1995;**34**:5949
- [57] Goetzberger A, Knobloch J, Voss B. *Crystalline Silicon Solar Cells*. Chichester, UK: John Wiley & Sons Ltd; 1998
- [58] Inslee J, Hendricks B. *Apollo's Fire: Igniting America's Clean Energy Economy*. 1st ed. USA: Island Press; 2009
- [59] Goetzberger A, Hebling C. Photovoltaic materials, past, present, future. *Solar Energy Materials and Solar Cells*. 2000;**62**:1-19

- [60] Antony A. Preparation and Characterisation of Certain II-VI, I-III-VI<sub>2</sub> Semiconductor Thin Films and Transparent Conducting Oxides. Kerala, India: Department of Physics, Cochin University of Science and Technology; 2004
- [61] Schubert MB, Werner JH. Flexible solar cells for clothing. *Materials Today*. Jan 6, 2006;**9**:42-50
- [62] Coonen S. Building Integrated Photovoltaics. Nov 15, 2017. Available from: [http://ayrintiteknolojileri.com.tr/yuklemedosyalari/file/duyurular/gunesenerjisi/ORNL-Coonen\\_BIPV.pdf](http://ayrintiteknolojileri.com.tr/yuklemedosyalari/file/duyurular/gunesenerjisi/ORNL-Coonen_BIPV.pdf)
- [63] Riha SC, Koegel AA, Emery JD, Pellin MJ, Martinson ABF. Low-temperature atomic layer deposition of CuSbS<sub>2</sub> for thin-film photovoltaics. *ACS Applied Materials & Interfaces*. Aug 2, 2017;**9**:4667-4673
- [64] Hamann TW, Martinson ABF, Elam JW, Pellin MJ, Hupp JT. Atomic Layer Deposition of TiO<sub>2</sub> on Aerogel Templates: New Photoanodes for Dye-Sensitized Solar Cells. *The Journal of Physical Chemistry*. 2008;**112**:10303-10307

IntechOpen